An Intermediate Complexity Model for El Niño Southern Oscillation

Ruth Musgrave
Supervisor: Dr Simon Clarke
Co-Supervisor: Dr Richard Wardle

Honours Thesis submitted as part of the B.Sc (Honours) degree in the School of Mathematical Sciences, Monash University.

Date of submission: 20.10.08

Acknowledgements

First and foremost I would like to thank my supervisor, Simon, not only for initiating my interest in this topic in the first place, but for his patience, guidance and encouragement over the duration of this project. His good humoured nature combined with a few well timed words of encouragement have kept me motivated throughout the year. Thanks so much Simon!
I would also like to thank all the staff and students with whom I have had the pleasure of interacting over the past two years in the School of Maths. I've been surrounded by some truly lovely people and it's been a great experience.
Last, but certainly not least, I would like to thank Lee for his love, support and shell-scripts.

Abstract

An Intermediate Complexity Model for El Niño Southern Oscillation is created using an established linear 1.5 layer ocean and sea surface temperature model and coupling it to a Gill-type atmosphere model. The model exhibits ongoing oscillations in both sea surface temperature and zonal wind anomalies arising solely from the interactions of the coupled ocean-atmosphere system. The oscillations have ENSO-like amplitudes and timescales and show a tendency to be seasonally locked. Variations of model parameters demonstrate that the nature of the oscillation is strongly dependent upon the strength of coupling between the ocean and atmosphere. Changes in the background climatology show that the coupling is modified by the progression of the seasonal cycle. It is suggested that the tendency for ENSO to be seasonally locked arises from the changes in the coupling in different regions of the Pacific at different times of the year. Possible dynamical mechanisms for ENSO are examined.

Contents

1 Introduction

The name "El Niño" ("The Christ Child") was first coined by Peruvian sailors and fishermen in relation to a warm current observed every few years around Christmas time. It was noted in a series of publications during the 1890s in the newly created *"Boletin de la Sociedad Geográfica de Lima"* the that this warm current, the *"contracorriente El Niño"*, appeared to be associated with torrential rains in the usually dry regions of north-western Peru. The phenomenon generated considerable interest amongst Peruvian scientists and was even reported in London in 1895, however at the time it was considered to be little more than a regional geographic curiosity and consequently received little international attention.

Interest in the Peruvian phenomenon was not reignited until the 1920s, when the large El Niño event of 1925-1926 caught the attention of U.S. naturalist Robert Murphy who happened to be in Peru at the time. Murphy organised the large scale observation of the event across Peru and was responsible for the first coherent picture of the larger scale effects of an El Niño event. Concurrently, working on (what appeared to be) an entirely separate problem in India, British scientist Sir Gilbert Walker noted a "Southern Oscillation" in atmospheric pressures over the Pacific basin. Rising pressures in the eastern Pacific seemed to be associated with falling pressures in the west, and vice versa. The timescale of the oscillation was around four years, though in some cycles the oscillation was more apparent than others. Walker further noted that certain phases of the oscillation brought drought to regions of Australia, Indonesia, India and parts of Africa, and he postulated that the weather in these regions was somehow linked to the pressure oscillation over the Pacific Ocean.

It was not until several years later however, in 1929, that the crucial link between the Peruvian coastal phenomenon of El Niño and Walker's Southern Oscillation was drawn when a Dutch scientist, Hendrik Petrus Berlage, Jr. noticed a correspondence between Gilbert Walker's Southern Oscillation and Murphy's observations of the 1925 event. Berlage obtained a chronology of precipitation anomalies in northern Peru since the turn of the century, and noted that El Niño events corresponded to times of high pressure anomalies in the Eastern Pacific, and low pressure anomalies in the western Pacific, i.e. specific phases of the Southern Oscillation.

Observations through the mid-twentieth century confirmed that the El Niño Southern Oscillation was a large scale phenomenon with far-reaching effects on the weather. El Niño was recognised to be only one phase of a continuing oscillation of the Pacific ocean and atmosphere, the complementary phase being dubbed "La Niña" which is characterised by somewhat cooler sea surface temperatures in the eastern Pacific. A further breakthrough in understanding the phenomenon came in 1969 when a Norwegian-American meteorologist, Jacob Bjerknes, identified positive feedbacks arising between the coupled ocean and atmosphere that serve to enhance initial small scale anomalies. The Bjerknes hypothesis has become an enduring paradigm for understanding the interaction of the coupled ocean and atmosphere across the Pacific.

Since the advent of numerical models in the 1980s, considerable progress has been made in understanding the dynamics of the oscillation. Simple physical models can be quickly built and tested, allowing new ideas to be verified against observation. The TOGA decade (Tropical Ocean and Global Atmosphere) between 1985 and 1994 saw a huge increase in available observational data as permanent buoys were installed across the zonal extent of the equatorial Pacific.

The El Niño event of 1997-1998 was particularly strong, and brought the phenomenon to the attention of the public at large. It was during this event that the term "El Niño" became synonymous with extreme weather events, and not without reason for the effects of El Niño are now known to include droughts in places as geographically distant as South America, India, and Australia as well as flooding in regions of South America and Cuba that are usually desert. It is El Niño's reputation for unusual and often extreme weather events having the potential to cause devastation in some of the world's most economically fragile communities that makes it so important to understand the mechanism behind the oscillation so that it may be possible to to make predictions about future events.

Of particular influence and contribution in ENSO research have been a class of simple numerical models known as *intermediate complexity models* (ICMs). These models use appropriate simplifications and approximations to the underlying physics of the ocean and atmosphere to recreate the dynamics of the oscillation. This thesis details a project which aimed to create such an ICM, and explores some of the dynamical underpinnings of ENSO. In Section 2, an outline of the fluid dynamics of the tropical ocean and atmosphere is given. Section 3 discusses intermediate complexity models for ENSO, with particular emphasis on the Zebiak-Cane model, the first ICM to successfully reproduce ENSO-like oscillations. Section 4 gives an overview of a simple ocean and sea surface temperature model (GModel) developed at the Netherlands Centre for Climate Research which was used as a basis for the ICM of this work. Section 5 describes the development of a physical Gill-type atmosphere model, and its integration into GModel to create a fully coupled ocean-atmosphere model for ENSO. Section 6 shows the results of a 'standard' 50 year run of the coupled model. Section 7 discusses the impact of changing parameter values of the model, and the sensitivities of the model to changes in the background state arising from seasonal variations. Also in this section is a brief exploration of the effects of different types of initialisations to the model on the subsequent development of model anomalies. Section 8 discusses the possible dynamical underpinnings of the model oscillation, and Section 9 summarises the work undertaken in this project, and the potential for future work possible with this model.

2 Fluid dynamics of ENSO

ENSO occurs as a result of the interaction of the equatorial Pacific Ocean with the overlying atmosphere. The interaction is modulated by sea surface temperatures which respond to ocean currents that are in turn generated by wind stresses at the surface of the ocean. Positive feedbacks arising through these interactions can result in the growth of perturbations which are manifested as peaks in the ENSO cycle. Thus, ENSO is observed to be an oscillation around a mean background state of the equatorial Pacific ocean and atmosphere.

2.1 The background state of the equatorial Pacific

Uneven solar heating of different latitudes results in increased warming and evaporation over equatorial regions. Rising air in these regions causes the equatorwards flow of surface air from mid-latitudes towards the equator, creating the lower atmospheric component of the Hadley circulation. The rotation of the earth means that air travelling towards the equator gains an easterly component as a direct consequence of the principal of conservation of angular momentum. As a result, upon reaching the equator, winds have a significant easterly component and these easterly winds along the equator are known as the Trade Winds.

The action of the Trades on the equatorial Pacific is to blow the warm, buoyant surface waters towards the west where a mass of warm water builds up, suppressing the thermocline (often defined as the 20° isopyncal) and raising the sea surface temperature and sea surface height there. The Coriolis effect means that wind driven surface currents in the ocean have a component that is directed to the right of the wind stress in the northern hemisphere, and to the left of the wind stress in the southern hemisphere. This results in a mean upwelling along the equator as the easterly Trade Winds induce oceanic currents with a poleward component. In the eastern Pacific, the shallower thermocline means that the upwelling water is cool resulting generally lower sea surface temperatures compared to those in the west.

Positive feedback arises as the warmer sea surface temperatures of the western Pacific drive evaporation and rising air in the atmosphere above the region. As the air rises, a low pressure region is created and convergent surface winds are induced. A complementary process occurs in the eastern Pacific where cool sea surface temperatures result in atmospheric subsidence and sinking. A high pressure region forms and divergent surface winds are created. The result is an enhancement to the easterly Trade Winds, with the overall atmospheric equatorial circulation being known as the Walker Circulation.

ENSO is observed to be a cyclical perturbation to this mean state as the Walker Circulation strengthens and weakens. El Niño is characterised by an anomalous weakening in the Walker Circulation and an associated rise in sea surface temperatures in the eastern Pacific by up to 3°. Complementary La Niña is identified as a

strengthening of the Walker Circulation, and cooler sea surface temperatures in the east.

The basic mechanism of the oscillation may be understood in terms of three components: the ocean; the atmosphere and the sea surface temperature. By making appropriate physical approximations to the exact equations of motion for each, the important physical processes underlying the phenomenon may be examined.

2.2 The ocean

The momentum balance equation for a fluid with a constant density in a rotating frame is given:

$$\frac{D\mathbf{u}}{Dt} + \frac{1}{\rho}\nabla p + g\hat{z} = -2\boldsymbol{\Omega} \times \mathbf{u} - \boldsymbol{\Omega} \times \boldsymbol{\Omega} \times \mathbf{r} + \mathcal{F} \tag{2.2.1}$$

Where $D\mathbf{u}/Dt$ is the Lagrangian acceleration (following the fluid flow), ρ the fluid density, p the pressure, g the gravitational acceleration, Ω the rotation rate of the frame, $\mathbf{r}$ the position vector of the fluid and $\mathcal{F}$ the friction acting on the fluid parcel. Thus, a fluid's acceleration is largely governed by four distinct forces: the pressure gradient force, the gravitational force, forces arising from rotation (the Coriolis and Centrifugal forces) and frictional forces (including viscous effects and surface stresses). Observational evidence suggests that ENSO is contained within a region that is much larger in zonal extent than in meridional, as such, it is appropriate to approximate the Coriolis term by a term that varies linearly with distance from the equator. Such a beta-plane model still captures the essential rotational effects on the system whilst allowing the equations to be solved more simply.

In order to model the motions of the thermocline and upper ocean in ENSO models, the equations of motion are solved for a buoyant shallow layer above a deep, stationary lower layer (Dijkstra and Burgers [2002]). The hydrostatic approximation is applied in both layers with the consequence that horizontal velocities are depth independent, and the vertical momentum equation becomes the hydrostatic equation. As there are no vertical gradients in horizontal velocities, it is possible to integrate over the upper layer having a variable depth h and appropriate boundary conditions to obtain the following reduced gravity equations:

$$\frac{\partial u}{\partial t} + u\frac{\partial u}{\partial x} + v\frac{\partial u}{\partial y} - \beta_0 y v = -g'\frac{\partial h}{\partial x} + \frac{\tau_0 \tau^x}{h\rho} + A_H \nabla_H^2 u \tag{2.2.2a}$$

$$\frac{\partial v}{\partial t} + u\frac{\partial v}{\partial x} + v\frac{\partial v}{\partial y} + \beta_0 y u = -g'\frac{\partial h}{\partial y} + \frac{\tau_0 \tau^y}{h\rho} + A_H \nabla_H^2 v \tag{2.2.2b}$$

$$\frac{\partial (h)}{\partial t} + \frac{\partial (uh)}{\partial x} + \frac{\partial (vh)}{\partial y} = 0 \tag{2.2.2c}$$

Here, $g' = g\Delta\rho/\rho$ is the reduced gravity which accounts for the effect of the denser lower layer on the upper layer. The vertical friction term is replaced by a term for

the wind stress on the upper surface of the layer, $\tau_0\tau^x$, and the horizontal friction is given by a harmonic term, with an eddy viscosity A_H. The use of a large eddy viscosity rather than a molecular viscosity for sea water means that turbulent effects are neglected by this model. That $g' \ll g$ means that height perturbations to the top of the layer (i.e. the free surface) are much smaller than height perturbations to the interface between the two layers. As such, wave solutions to these equations often only show a small signature in the ocean surface height, but a much larger signature in the thermocline perturbation.

The instantaneous small amplitude response of the ocean to an applied wind stress may be found directly by considering an Ekman balance within the upper layer. This response may in general be well approximated by a sum of the free modes of the system. Hirst [1985] found that the subsequent evolution of the perturbation would then be dominated by the free mode having the largest growth rate (or smallest decay rate). As a result, the ocean response to a changing wind stress may be considered to be a superposition of free modes representing the adjustment of the ocean to earlier wind stresses, and a quasi-steady response to the instantaneous forcing. Hirst demonstrated that for realistic wind fields and couplings between the ocean and atmosphere, Kelvin and Rossby wave are destabilised in the ocean. As such, the oceanic response may be considered in two parts: the unforced solutions arising from perturbations to the system, and the forced solutions arising from the instantaneous wind stress.

Considering first the unforced, non-dissipative equations linearised around a stationary mean state with a constant layer thickness, H, a set of equations admitting equatorial Kelvin and Rossby wave solutions are obtained:

$$\frac{\partial u}{\partial t} - \beta_0 y v = -g' \frac{\partial h}{\partial x} \tag{2.2.3a}$$

$$\frac{\partial v}{\partial t} + \beta_0 y u = -g' \frac{\partial h}{\partial y} \tag{2.2.3b}$$

$$\frac{\partial h}{\partial t} + H\left(\frac{\partial u}{\partial x} + \frac{\partial v}{\partial y}\right) = 0 \tag{2.2.3c}$$

h is the perturbation height of the layer. Equatorial Kelvin waves are non-dispersive and propagate eastwards along the equator. They have no meridional velocity component, and their zonal velocity gives rise to a meridional balance between the Coriolis force and a pressure gradient force arising from an exponentially decaying height structure with a peak at the equator. Their meridional length scale is of order the Rossby radius ($\approx 300\ km$) and they have a group velocity of around 2 ms^{-1}.

Rossby waves are also admitted by the above set of equations. Of particular relevance to ENSO are the lower order solutions having off equatorial maxima at low latitudes. These are dispersive waves having both zonal and meridional velocity components. They propagate westwards, with the lowest order wave having a group velocity that is approximately one third that of a Kelvin wave.

The instantaneous, forced response of the ocean to an applied wind stress is found by again linearising Equations 2.2.2, and assuming an instantaneously steady response. The harmonic friction term may be approximated for an atmospheric forcing of order the Rossby radius:

$$A_H \nabla_H^2 u \approx -\frac{2A_H u}{\lambda_0^2} \approx -a_m u \tag{2.2.4}$$

The equations of the forced response become:

$$a_m u_E - \beta_0 y v_E = \frac{\tau_0 \tau^x}{\rho H} \tag{2.2.5a}$$

$$a_m v_E + \beta_0 y u_E = \frac{\tau_0 \tau^y}{\rho H} \tag{2.2.5b}$$

$$w_E = H\left(\frac{\partial u_E}{\partial x} + \frac{\partial v_E}{\partial y}\right) \tag{2.2.5c}$$

By continuity, horizontal velocity gradients give rise to the vertical velocity in Equation 2.2.5c, and it is in this manner that cool water from below the thermocline may be drawn into the upper layer, or warm water from the upper layer pumped down towards the thermocline. This Ekman pumping plays an important role in modulating the sea surface temperature, and non-linearities in the mechanism are important in the dynamics of a self-sustaining model for ENSO.

The reduced gravity equations for a 1.5 layer ocean are derived in Appendix A.

2.3 The atmosphere

As with the ocean, the governing equation for motions in the atmosphere is given by Equation 2.2.1, though this time the forcing term must is for atmospheric heating by sea surface temperatures. Once again, a beta-plane approximation is appropriate given the ratio of the observed meridional to zonal extent of the phenomenon. However, unlike the ocean it is not necessary to consider a two layer atmosphere. The atmosphere, having less inertia than the ocean, responds quickly to changes in the ocean but does not provide large scale adjustment to the system. Atmospheric perturbations are localised around regions of warm or cool sea surface temperature but their evolution independent of the ocean is not crucial to the oscillation. As such, a simple one layer shallow water model with linear damping is sufficient for the low level response of the atmosphere in the tropical Pacific. The equations are given below:

$$\frac{\partial u_a}{\partial t} - \beta_0 y v_a - \frac{\partial \Theta}{\partial x} + a_M u_a = 0 \tag{2.3.1a}$$

$$\frac{\partial v_a}{\partial t} + \beta_0 y u_a - \frac{\partial \Theta}{\partial y} + a_M v_a = 0 \tag{2.3.1b}$$

$$\frac{\partial \Theta}{\partial t} - c_a^2\left(\frac{\partial u_a}{\partial x} + \frac{\partial v_a}{\partial y}\right) + a_M \Theta = Q \tag{2.3.1c}$$

Where Θ represents the geopotential height and c_a is the Kelvin wave speed in the atmosphere ($\approx 60\ ms^{-1}$). Analytic solutions to Equations 2.3.1 were studied by Gill [1980] and so models of this class are known as Gill Models. The atmosphere is forced by a heating term, Q, which in its simplest form is linearly related to the sea surface temperature. Though non-linearities in the heating parametrisation lend more accuracy to the calculated winds compared to observation, these are not crucial to the ENSO oscillatory mechanism (Battisti and Hirst [1988]). The perturbation model response gives a convergent wind field over areas of warm sea surface temperature anomalies, and a divergent response over cool sea surface temperature anomalies. Of most importance to ENSO are the westerly winds that arise to the west of a region of warm sea surface temperature, and the easterly anomalies to the east. It is these winds that can provide positive feedbacks to the system under some circumstances they enhancing sea surface temperature perturbations and causing the build up of a warm or cool event in the eastern Pacific.

2.4 The sea surface temperature

Most generally, the sea surface temperature is governed by an advection-diffusion equation which accounts for the redistribution of heat energy by both molecular motion (diffusion) and large scale fluid motions (advection):

$$\frac{\partial T}{\partial t} + \mathbf{u}.\nabla T = K_H \nabla_H^2 T + K_V \frac{\partial^2 T}{\partial z^2} \tag{2.4.1}$$

The upper layer of the ocean is considered to be well mixed and reasonably vertically homogeneous up to a depth of around $50m$. Thus, for the purposes of establishing the sea surface temperature it is necessary to consider only the advection of fluid and diffusion of heat across the boundaries of this layer. Assuming the temperature is constant within the layer, then integrating over its depth, H_m, and imposing appropriate boundary conditions for the temperature gradient at each surface (see, for example, Dijkstra [2005]), Equation 2.4.1 may be written:

$$\frac{\partial T}{\partial t} + u\frac{\partial T}{\partial x} + v\frac{\partial T}{\partial y} = K_H \nabla_H^2 T + \frac{Q_{oa} - Q_b}{\rho C_p H_m} \tag{2.4.2}$$

Where Q_{oa} represents the heat flux across the ocean-atmosphere interface, and Q_b is the heat flux through the bottom interface of the layer. C_p is the heat capacity of seawater. It is clear that the temperature of the layer is governed by both horizontal advective processes and heat fluxes across the upper and lower boundaries to the layer.

At the upper interface between the atmosphere and ocean, the heat flux is diffusive and may be parametrised by a simple, linear damping term:

$$\frac{Q_{oa}}{\rho C_p H_m} = -a(T - T_r) \tag{2.4.3}$$

Where T_r is a reference atmospheric equilibrium temperature.

At the lower interface between the well mixed layer and the shallow water layer, the heat flux will be dominated by vertical advection. Thus an appropriate parametrisation is:

$$\frac{Q_b}{\rho C_p H} = w\frac{T - T_s}{H_u} \tag{2.4.4}$$

In this, T_s is the subsurface temperature of the shallow water layer, and H_u is the depth at which this subsurface temperature is defined. The vertical temperature gradient depends upon the position of the thermocline (becoming larger in the vicinity of the thermocline), therefore the heat flux into the bottom of the layer is affected by variations in the thermocline depth.

Vertical velocities into the base of the mixed layer may arise by two processes: Ekman pumping (Equations 2.2.5) and thermocline displacements arising due to the propagation of waves (Equations 2.2.3). Both processes contribute non-linearities to the sea surface temperature equation. For example, Ekman pumping will only affect the sea surface temperatures when it results in upwelling water which brings cool water from below the thermocline up to the surface layer. Furthermore, there is a maximum cooling that Ekman upwelling may attain that is governed by the temperature of the sub-thermocline water. Motions of the thermocline also have non-linear effects on the sea surface temperature as the maximum cooling attainable due to a raised thermocline is simply the temperature of water below the thermocline, and the maximum heating resulting from a lowered thermocline is simply the temperature of the mixed layer. Both Ekman pumping and thermocline motions are subject to a further non-linearity arising from the background state of the Pacific. The lowered thermocline in the western Pacific means that the effectiveness of both processes is much reduced there as cooler, sub-thermocline water is too far below the surface of the ocean to be entrained. By similar reasoning, these processes are much more effective in the eastern Pacific where the thermocline is shallow and cool water lies close to the surface of the ocean.

The non-linearities present in the sea surface temperature equation are able to prevent the run-away growth of a coupled linear atmosphere and ocean by providing saturation effects in the maximum temperature anomalies attainable. Their presence in the delayed oscillator conceptual model of Battisti and Hirst [1988] is crucial to ongoing, stable oscillations, and as such, they are often included in otherwise entirely linear intermediate complexity models for ENSO.

2.5 Coupling

The coupling between the ocean and atmosphere describes the amount by which ocean SST anomalies force atmospheric wind anomalies and vice versa. In coupling the atmosphere model to the ocean, anomalous velocities are converted to 'effective' wind stresses which accounts for wind energy lost to other processes such as turbulence. The effective wind stresses are used to drive the ocean model, and their

magnitude is determined by a drag coefficient, ζ. Increasing ζ causes the wind to force the ocean more efficiently. The amount by which the ocean forces the atmosphere is determined by the heating parametrisation, which, in simple models is the proportionality constant in a linear relation between the temperature anomaly and heating.

Depending upon the exact nature of the model, other factors also may indirectly affect the coupling. For example, reducing the mean depth of the thermocline would cause height perturbations to have more effect on the sea surface temperature, in effect causing a greater SST anomaly for the same amount of wind stress forcing.

It is the coupling between the ocean and atmosphere that gives rise to important feedback mechanisms which, under the right conditions, can lead to the growth of small scale perturbations within the model.

2.6 Feedbacks

The interaction of the coupled ocean and atmosphere gives rise to three important feedback mechanisms which are responsible for the growth of small perturbations in the central Pacific into the large scale anomalies observed at the peak of El Niño and La Niña events (Neelin [1990]). These three mechanisms are described below:

1. Thermocline feedback: A warm sea surface temperature anomaly occurring in the central to eastern Pacific causes warm air to rise above the anomaly resulting in a convergent surface wind field. The westerly winds induced to the west of the warm SST are manifested against the background easterly Trade winds as an anomalous weakening, with the result that the wind stress responsible for piling up warm water in the western Pacific and causing the thermocline to be deepened there is reduced. As a result, the thermocline in the western Pacific rises slightly, and warm water travels east causing the thermocline to be deepened there. In the region of the original SST anomaly, the thermocline is deepened causing the subsurface temperature, T_s, to effectively increase. Downwelling results in $w > 0$, and for $T_s > T$, equation 2.4.4 gives $Q_b < 0$. By equation 2.4.2, $\partial T/\partial t \approx -Q_b$, thus there is an increase in the SST in that region.

2. Upwelling feedback: Once again, a warm SST anomaly in the central to eastern Pacific results in a weakening of the background easterly winds overlying the equatorial region. The wind stresses in Equations 2.2.5 (which are also valid for the background response of the ocean to the Trade winds) are reduced, and consequently the induced Ekman velocities are less. By continuity, this results in reduced upwelling along the equator, which causes less cool subsurface water to be drawn into the upper mixed layer, resulting in an amplification of the original warm SST anomaly. The timescale upon which this process occurs is much shorter than that for the thermocline feedback, and to first order each process may be considered separately.

3. Zonal advection feedback: This arises by the zonal advection of warm water by zonal currents. A warm anomaly in the central/eastern Pacific induces westerly wind anomalies to the west of it. The westerly wind anomalies induce eastward currents due to both Ekman processes and wave dynamics, resulting in $u > 0$. The temperature gradient across the zonal length of the Pacific tends to be $\partial T/\partial x < 0$. Equation 2.4.2 shows that $\partial T/\partial t \approx -u\,\partial T/\partial x$, thus for a negative temperature gradient and positive zonal flows, the temperature in the region of the original anomaly increases.

These mechanisms amplify perturbations to the sea surface temperature in the Pacific, resulting in instabilities of the coupled system. The sea surface temperature equation of Section 2.4 may include non-linearities to prevent the runaway growth of perturbations under the influence of these feedbacks. Both the feedback mechanisms and the non-linearities in the sea surface temperature equation are important in understanding the dynamics behind the ENSO phenomenon.

3 Intermediate Complexity Models for ENSO

Intermediate complexity models are a class of numerical models that combine simple physical models of the ocean, atmosphere and sea surface temperature into a coupled model for the equatorial Pacific. Suitable physical approximations allow the models to be simplified such that they still contain the essential ingredients required to produce an ENSO like oscillation, without being unnecessarily computationally expensive. Because the models can be run relatively quickly on ordinary computers, parameter spaces can be easily explored and the relative importance of difference physical mechanisms may be evaluated. One of the key distinctions between intermediate complexity models and more elaborate models such as general circulation models is that the former do not attempt to model the background flows of the system. Rather, perturbation equations are constructed such that all quantities computed are anomalies, and if necessary, observed background climatologies are used for the mean flows.

3.1 The Zebiak-Cane model

One of the most influential ICMs in the development of ENSO theory was that created by Zebiak and Cane [1987] which combines simple models of the ocean, atmosphere and sea surface temperature to produce a model capable of producing on-going oscillations in the sea surface temperature in the eastern Pacific with a period of three to four years. The model components are briefly described below with reference to Section 2.

1. The ocean: Zebiak and Cane (hereafter ZC) consider a linearised 1.5 layer reduced gravity model in which a mixed layer been embedded into the shallow water layer. The ocean basin used is rectangular, extending from 124°E to 80°W, and boundary conditions are for no mass flux through the western boundary and no zonal flow through the east. The reduced gravity equations of Section 2.2 are used to calculate the mean velocities within the shallow water layer, however for the purposes of calculating the sea surface temperature, it is helpful to know the flows into and through the mixed layer alone. In order to estimate these flows, ZC explicitly calculate the velocities arising solely from Ekman processes. As Ekman processes are generally confined to the very upper layer of the ocean (the mixed layer), it is reasonable to then assume that the difference between the velocities in the mixed layer and the mean velocities of the shallow layer arise entirely from these Ekman processes. As such the velocities in the mixed layer may be found.

2. The atmosphere: A Gill model as presented in Section 2.3 is used, but the heating term is now composed of two non-linear parts, one corresponding to diabatic heating by the sea surface temperature anomaly, and the other corresponding to a latent heating resulting from the background moisture convergence of the low lying wind field. The diabatic heating term is given below:

$$Q_d = \alpha T \exp[(\bar{T} - 30)/16.7] \tag{3.1.1}$$

where $\bar{T}$ is the background temperature specified by the climatology, and T is the SST anomaly. This heating term means that areas with a warmer background temperature heat the atmosphere more effectively than those areas with cooler background temperatures. The latent heating term is given:

$$Q_l^{n+1} = \beta[M(\bar{c} + c^n) - M(\bar{c})] \tag{3.1.2}$$

Where

$$M(x) = \begin{cases} 0, & x \leq 0 \\ x, & x > 0 \end{cases}$$

The latent heating at iteration $n+1$ is determined by c^n, the anomalous surface wind convergence at iteration n, against the climatological background convergence, $\bar{c}$. It is only active when the total wind field is convergent and warm moist air is being brought into the region above the warm SST where it condenses releasing latent heat into the atmosphere. Zebiak [1982] found that by including such a moisture convergence term the atmospheric response to SST anomalies was focused in regions of mean background convergence in agreement with observations of wind anomaly patterns during ENSO.

3. The sea surface temperature: Using the mixed layer velocity anomalies, ($\mathbf{u_m}$), and the Ekman upwelling into the mixed layer, w_m, determined by the ocean model, ZC use the following equation to find the sea surface temperature anomalies:

$$\frac{\partial T}{\partial t} = -\bar{\mathbf{u}}_\mathbf{m}.\nabla T - \mathbf{u_m}.\nabla(\bar{T} + T) - [M(\bar{w}_m + w_m) - M(\bar{w}_m)]\bar{T}_z \\ - M(\bar{w}_m + w_m)T_z - \alpha_s T \tag{3.1.3}$$

Where $M(x)$ is as defined for the atmosphere and overbars denote climatological mean values. The first two terms account for the horizontal advection of temperature by mean and anomalous currents. Temperature flux into the bottom of the mixed layer is parametrised in the next two terms, with $\bar{T}_z$ being a prescribed vertical temperature gradient, and T_z an anomalous gradient dependent upon the thermocline depth. T_z reaches a saturation when the thermocline is particularly shallow or deep, reflecting the fact that thermocline movements cannot cause the SST to become cooler than the sub thermocline water, or warmer than the surface water. The final term in Equation 3.1.3 represents heat loss through the sea surface to the atmosphere.

ZC combined the above three components into a single model which they initialised with an imposed westerly wind anomaly in the central western Pacific. The anomaly was held fixed for the first four months of the run after which time the coupled model was continued for a 90 year run. During this time sustained oscillations in sea surface temperature in the eastern Pacific were observed, arising solely from the self-interactions of the coupled system. The oscillations were somewhat irregular, having a period of 3-4 years and a tendency for larger amplitude warm events than cool events. ZC also noted a tendency for warm events to occur either in June or around the end of the year. Associated with peak SST anomalies in the eastern

Pacific were large-scale equatorial westerly wind anomalies arising from positive feedbacks between the ocean and atmosphere. All of these features are in agreement with observations of ENSO, and the model was breakthrough in understanding the dynamics of the phenomenon.

ZC found that their oscillation was robust to changes in parameters over a range of physical values. Key sensitivities occurred in changes to parameters that amounted to a change in the coupling strength between the ocean and atmosphere (such as increasing the wind stress per unit wind velocity, or heating per unit SST anomaly). Reducing the coupling strength caused the oscillation to have a smaller amplitude and shorter period and below a critical coupling, the oscillation ceased to occur. Increases in the coupling strength resulted in a longer period oscillation with large amplitude. ZC also investigated the effects of the background climatologies on the model oscillation and found that stopping the progression of the seasonal cycle at different points of the oscillation strongly affected its subsequent evolution. Different background states arising from the seasonal cycle modified the effective coupling strength of the system, with mid-year conditions having a stronger coupling and being particularly favourable for the development of anomalies. However, progression of the seasonal cycle was not found to be critical to the oscillation as it still occurred with the background conditions fixed, though it had less variability than when the seasonal cycle was allowed to progress.

In all, three major physical processes important to the ENSO cycle were identified by this early model. Positive feedbacks resulting the amplification of perturbations in the atmosphere and ocean under certain conditions, non-linear effects preventing the perturbations from growing unphysically large under the influences of positive feedbacks, and a systematic delay between changes in the eastern Pacific and the equatorial wind stress.

4 GModel-3.0

GModel is an equatorial coupled atmosphere and ocean model that, in its most recent version, has been developed by Gerrit Burgers at the Netherlands Centre for Climate Research. It is composed of three components:

1. A linear, 1.5 layer shallow water ocean model with domain 30°S - 30°N, 122°E - 292°W and realistic boundaries.
2. A simple sea surface temperature equation valid for the central and eastern Pacific.
3. An atmosphere component which can either be coupled to the ocean using a statistical atmosphere model, or used to force the ocean with observed wind stress data.

The equations for each model component are solved using finite differences on a grid with a resolution of 2° in the zonal and 1° in the meridional directions and a timestep of 8 hours. The model may be run either in 'forced' or 'coupled' modes. In the coupled mode, a statistical atmosphere creates regression patterns of observed wind stress anomalies to observed sea surface temperature anomalies in the Nino-3 and Nino-4 regions (Burgers and Oldenborgh [2003]). These regression patterns are then combined with noise and used during the run to calculate the likely atmospheric response to model SST anomalies. In the forced mode, the ocean is driven by Florida State University (FSU) wind pseudostress data between 1966 and 1999 and there is no feedback from the ocean to the atmosphere. Both modes result in ongoing, ENSO like oscillations of the ocean sea surface temperature and thermocline, however the atmosphere component in the coupled mode is an entirely empirical response. As such, the purpose of the first part of this work was to replace the empirical coupled atmosphere with a physically based model atmosphere. Details of the atmospheric model used are given in Section 5, whilst this section will concentrate on the two components of GModel that will be used: the ocean and the sea surface temperature models.

4.1 GModel: Ocean component

The ocean component is a 1.5 layer, linear model of a baroclinic mode on a beta plane (Burgers et al. [2002]). The equations are linearised versions of the reduced gravity equations 2.2.2 discussed in Section 2.2, but they allow an additional forcing of the thermocline by a heat source, Q:

$$\frac{\partial u}{\partial t} - \beta_0 y v + g' \frac{\partial h}{\partial x} + F_M(u) = X \tag{4.1.1a}$$

$$\frac{\partial v}{\partial t} + \beta_0 y u + g' \frac{\partial h}{\partial y} + F_M(v) = Y \tag{4.1.1b}$$

$$\frac{\partial h}{\partial t} + H\left(\frac{\partial u}{\partial x} + \frac{\partial v}{\partial y}\right) + F_H(h) = Q \tag{4.1.1c}$$

X and Y are wind pseudostress anomalies in the zonal and meridional component respectively, and these are the forcings on the horizontal momentum equations. The frictional terms, $F_M(u)$, $F_M(v)$ and $F_H(h)$, consist of fourth order, harmonic and linear parts. The harmonic part accounts for eddy viscosities and diffusivities in the fluid, whilst the linear part is only active near the northern and southern boundary of the basin and prevents the unphysical propagation of waves along these boundaries. The small, fourth order terms are used to suppress short wavelength numerical instabilities near the equator. The thermocline depth, H, is set to be a constant $150m$ throughout the zonal extent of the basin, neglecting the background tilt of the thermocline discussed in Section 2.1. However, this tilt is important to the dynamics of the model as the sea surface temperature is more readily affected by current on and height changes of a shallower thermocline than a deeper thermocline (Section 2.4). The tilt of the thermocline is therefore emulated in the sea surface temperature equation which includes longitude dependence in each term, resulting in different terms being dominant at different longitudes.

At each timestep, h, u and v are calculated as follows:

1. Integration of continuity equation: Velocities from the previous timestep are used with height dependent damping to calculate the new thermocline height at each grid point for this timestep.

2. Integration of u-momentum equation: Wind stress forcings and the gradient of the thermocline height are used with velocity dependent friction terms to calculate a a new value for the zonal velocity at each grid point for the new timestep.

3. Integration of v-momentum equation: Wind stress forcings and the gradient of the thermocline height are used with velocity dependent frictions terms to calculate a new value for the meridional velocity at each grid point for the new timestep.

The model differs from that used by Zebiak and Cane (Section 3.1) in that it does not include a mixed layer with explicit calculation of the mixed layer velocities. Observational evidence has suggested that an empirical linear relation between the surface wind and observed zonal surface velocities in the ocean is slightly more accurate than a dynamical relation derived from a 1.5 layer model, even with an Ekman layer included (Boulanger [2001]). As such, the sea surface temperature equation used by GModel does not use calculated Ekman velocities.

4.2 GModel: Sea surface temperature equation

The SST is determined by the thermocline height and wind stress anomaly at each grid point. The relation between SST and thermocline height is empirical, arising from the observation that the SST is linearly dependent upon the thermocline depth. Perturbations to the thermocline height have more effect in the eastern Pacific where

the thermocline is shallower, as such the linear term is multiplied by a longitude dependent term, $\alpha_{sst}(x)$. In the central Pacific, advection by zonal current anomalies dominates and in GModel this is modelled by a term that is linearly related to the zonal wind stress. It has been found that this is a more accurate indicator of the zonal surface currents than the average velocities calculated by a 1.5 layer model. This type of parametrisation means that zonal currents not directly related to the local wind stress are neglected, however, anomalous upwelling and evaporational effects are included to some extent. To account for the longitude dependence of this effect, wind stresses are multiplied by $\beta_{sst}(x)$ which has a maximum in the central Pacific. The final term in the SST equation is one parametrising the damping of anomalies by the atmosphere, and it is linearly related to the SST. Its longitude dependence is given by $\gamma_{sst}(x)$. The full equation is:

$$\frac{dT}{dt} = \alpha_{sst}(x)h(x,y) + \beta_{sst}(x)(\tau)^x(x,y) - \gamma_{sst}(x)T(x,y) \tag{4.2.1}$$

The values of $\alpha_{sst}(x)$, $\beta_{sst}(x)$ and $\gamma_{sst}(x)$ are have been tuned to produce ENSO like oscillations when the model is run using observed wind stress data. A plot of the longitude dependence of each term is given in Figure 1. Both the damping term

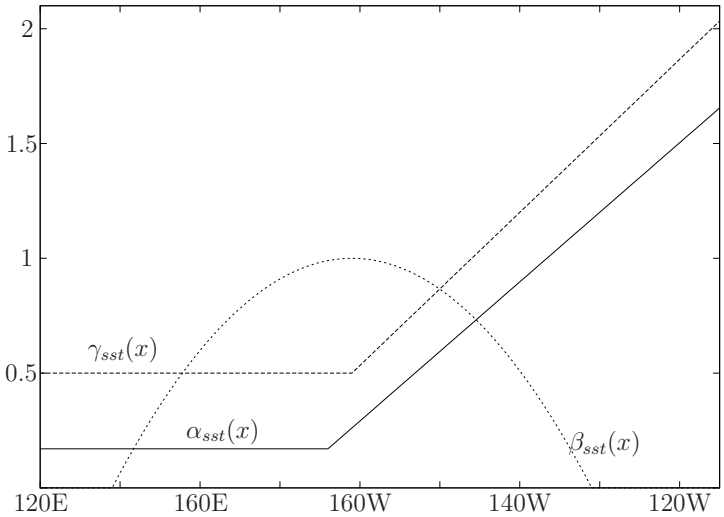

Figure 1: *Relative importance of factors in GModel SST equation as a function of longitude.* α_{sst} *is in units of K(10m)*$^{-1}$ *month*$^{-1}$, β_{sst} *in K (0.1 Pa)*$^{-1}$ *month*$^{-1}$, *and* γ_{sst} *in month*$^{-1}$

and the thermocline height term increase in importance in the eastern Pacific where the background state is such that temperature anomalies are quickly damped, and motions of the thermocline strongly affect the SST. The wind stress term is more important in the central Pacific where zonal currents and Ekman upwelling strongly affect the SST.

In this form, the sea surface temperature equation does not include the saturating non-linearity discussed in Section 2.4 and as a consequence, there is no mechanism in GModel to prevent the run-away growth of SST anomalies under the influence of positive feedbacks between the coupled ocean and atmosphere.

4.3 GModel: Results from forced run: 1966 - 1999

Without any modification, the model was run in 'forced' mode using Florida State University observed wind stress data between 1966 and 1999 to force the ocean component of the model. The SST was calculated diagnostically from the wind-induced currents. Figure 2 shows a time series of the SST anomalies in the NINO 3 region, defined to be between 5°N - 5°S and 150°W - 90°W, for both the anomalies calculated by GModel, and for observed anomalies in the same region.

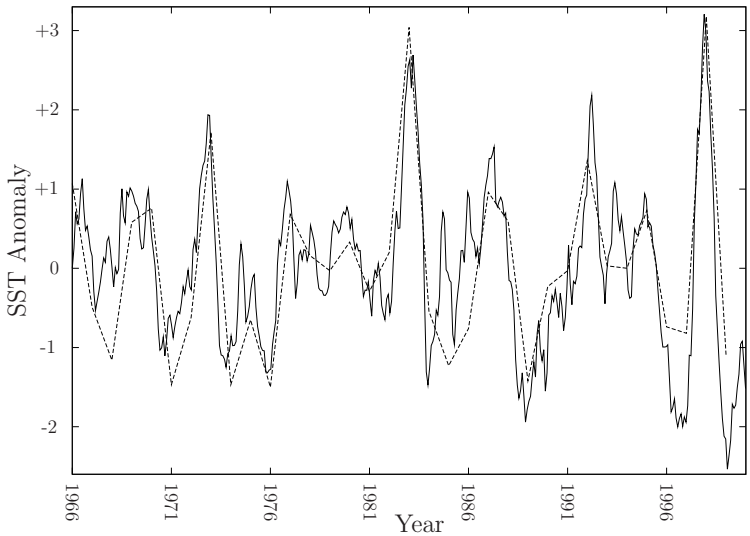

Figure 2: *NINO3 index of SST anomalies from GModel as forced by FSU observed winds between 1966 and 1999 (solid line), and observed SST anomalies (dashed line) between the same period from the NOAA Monthly Atmospheric and SST Indices data set*

The agreement between the observed SST anomalies and those calculated by GModel in response to observed wind stresses is very good. The observational data are yearly averages thus the time resolution is not as high as the GModel data, but the large scale pattern is still well replicated by the model. That the ocean and SST models used in GModel can reproduce anomalies to such accuracy despite the extensive simplifications and approximations used in their construction demonstrates their utility for understanding ENSO.

4.4 GModel: Ocean response to wind patch forcing

The model was forced by imposed westerly winds having a Gaussian velocity structure in both dimensions for one day, then allowed to relax with no further wind stresses acting on the model. The thermocline was initially flat, and snapshots of its subsequent evolution are contoured in Figure 3 after one month, three months, five months and seven months.

After one month the thermocline has become deeper in the region to the east of the initial wind stress, with a shallowing of the thermocline to the west. The regions of

the thermocline perturbation extend zonally beyond the region of windstress forcing, indicating propagation. The effects of wind stress forcing on the ocean are known to excite free modes, and it is possible to identify the eastwards propagating depressed thermocline perturbation as a downwelling Kelvin wave, and the off equatorial components of raised thermocline perturbations as possible upwelling and downwelling Rossby waves. The Kelvin wave speed is a parameter in the model having a value of $2.2ms^{-1}$, thus it takes approximately 50 days to cross the basin and reach the eastern boundary. By the end of three months, the downwelling wave has reached the eastern boundary and split into two coastal Kelvin waves, and a reflected gravest order Rossby wave. Rossby waves have a group velocity that is approximately one third that of Kelvin waves, and the reflected Rossby wave travels westward taking around five months to reach the western boundary. By the end of two years, the wave energy has largely dissipated and the thermocline is flat once again.

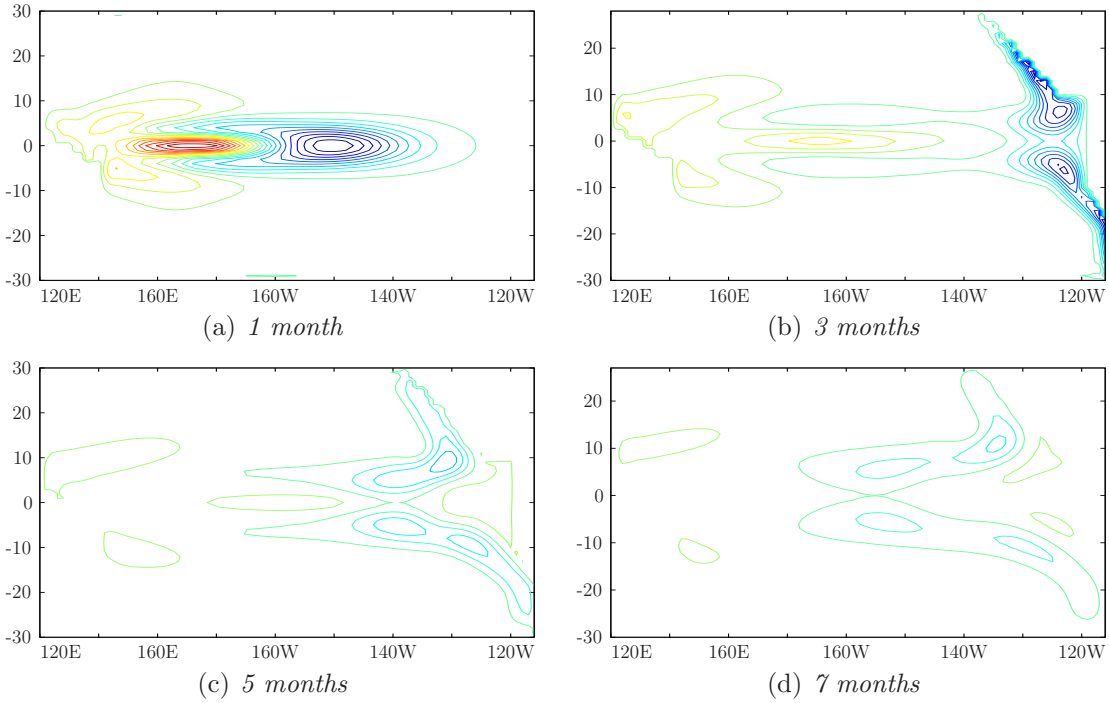

(a) *1 month* (b) *3 months*

(c) *5 months* (d) *7 months*

Figure 3: *GModel thermocline response to an impulse wind stress forcing in the central western Pacific occurring at t=0, after a) 1 month, b) 3 months, c) 5 months and d) 7 months. Perturbations have a maximum of 74cm and -77cm for upward (reds) and downward (blue) displacements respectively across all plots.*

5 Implementing a Gill atmosphere

In order to turn GModel into a fully coupled physically based model for the tropical Pacific ocean and atmosphere, it was necessary to replace the statistical atmosphere included in the model with a simple physical atmosphere. The atmosphere needed only to be capable of producing a sufficiently realistic low level wind response for ENSO simulations. A common atmosphere model used in this type of intermediate complexity model is a Gill model, named after Adrian Gill who described the analytic atmospheric response to some simple sea surface temperature distributions in 1980.

The model assumes that the heating rate is small enough that the equations of motion may be linearised. Dissipative effects are included in the form of a linear Rayleigh friction term (to account for momentum loss) and a linear Newtonian cooling term (to account for heat loss). For simplicity, the timescale for both processes is the same. The result is the following set of nondimensional momentum balance equations:

$$\epsilon u_a - \frac{y v_a}{2} = -\frac{\partial p}{\partial x} \tag{5.0.1a}$$

$$\epsilon v_a + \frac{y v_a}{2} = -\frac{\partial p}{\partial y} \tag{5.0.1b}$$

$$\epsilon p + \frac{\partial u_a}{\partial x} + \frac{\partial v_a}{\partial y} = -Q \tag{5.0.1c}$$

Where the length scale has been nondimensionalised by the equatorial Rossby radius:

$$(x^*, y^*) = (c_a/2\beta)^{1/2}(x, y), \quad t^* = (2\beta c_a)^{-1/2} t$$

u_a and v_a are atmospheric perturbation velocities, ϵ is a non-dimensional inverse time scale for Rayleigh friction and Newtonian cooling, c_a is the atmospheric Kelvin wave speed, p is pressure and Q is the heating of the atmosphere by the sea surface temperature anomaly. Equation 5.0.1c is derived by combining the vertical momentum equation (in this case the buoyancy equation) with the continuity equation, thus the set of equations simply describes the forcing of vertical velocities by heating, and the subsequent horizontal velocities at the surface arising by continuity of the fluid. The horizontal velocities are in geostrophic balance (with Rayleigh friction).

The equations are solved on a grid using finite differences with boundary conditions that the meridional velocity is zero at $y = \pm H$, where H is the maximum latitudinal height of the box. The numerical solution procedure is described in more detail in Appendix B.

5.1 Parametrising Q: Diabatic and latent heating

This simple atmospheric model is driven by the heating term, Q, which in its most basic form may be parametrised as being linearly dependent upon sea surface temperature anomalies. Zebiak [1982] proposed a numerical model in which Equations 5.0.1 are forced by a diabatic heating term arising by linearising the Clausius-Clapeyron relationship about the mean state sea surface temperature ($\bar{T}$):

$$Q = \alpha \Delta T (b\bar{T}^{-2}) e^{-b/\bar{T}} \tag{5.1.1}$$

ΔT is the SST anomaly, and α and b are constants. This form of heating parametrisation assumes that the dominant forcing for the model arises from evaporation at the sea surface, resulting in increased cumulus convection and atmospheric heating. Its functional form ensures that heating anomalies are more effective against a background of warm sea surface temperatures than cool.

Following Zebiak [1982], the model was reproduced for this current work in a stand alone version so that it could be easily verified against published results. Results for simple heating configurations centred both on and off the equator are shown in Figure 4.

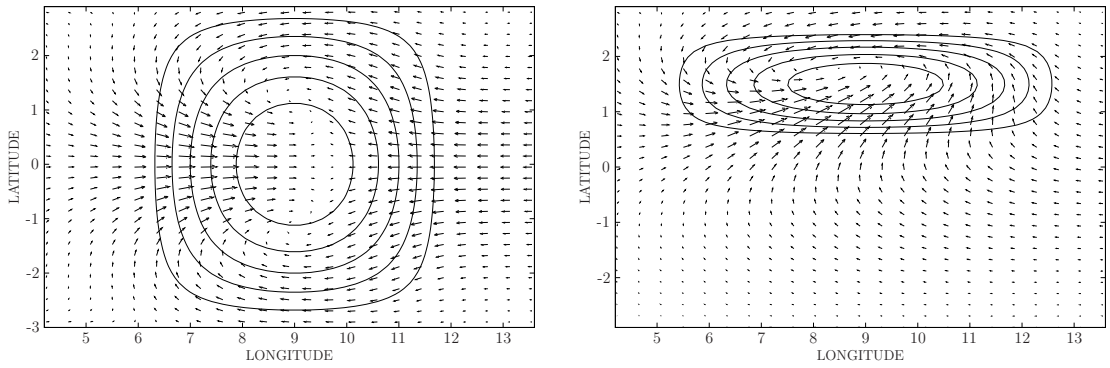

(a) *Centred equatorial heating* (b) *Off-equatorial heating response*

Figure 4: *Gill atmosphere response for heating parametrised by SST anomalies only. SST anomaly is positive and contoured, vectors denote wind response.* $\epsilon = 0.3$ *which corresponds to a decay timescale of* $\approx$*1 day. Latitude and longitude are dimensionless.*

Heating centred on the equator induces a meridionally symmetric response in the overlying winds which, for the simple heating distribution shown, is a superposition of a forced Kelvin wave and lowest order forced Rossby wave (Gill [1980]). The waves subsequently propagate eastwards and westwards, respectively, decaying with the rate $\epsilon = 1\,day$. Off-equatorial heating induces a cyclonic response to the west of the heating as rising air results in a low pressure region. The overall transport by the induced circulation is polewards as the Coriolis force is weaker closer to the equator thus geostrophic velocities are larger. In this case, the response is a superposition of the two lowest order Rossby waves.

Zebiak [1982] used observed sea surface temperature anomalies at different phases of an ENSO cycle to force the above model, and compared their results to observations of the wind fields at those times. He found that there was some large scale similarity between the model response and observations in regions of mean background convergence and along the equator, but that there were significant discrepancies particularly in the regions of the northeast and southeast Trades. Zebiak proposed that the model may be improved by including moisture convergence feedback in the heating parametrisation to account for latent heating by moist warm air in regions of net influx. The physical basis for this heating comes from the condensation of moisture from air that has been brought into a low pressure region. The change of state from vapour to liquid is associated with a latent energy release which causes atmospheric heating. This parametrisation takes into account both mean background convergence conditions, and induced "anomalous" convergence arising from wind anomalies due to the diabatic part of the heating. As such, it requires an iterative procedure to fully account for the anomalous convergence.

Zebiak [1986] implemented such a heating parametrisation. The heating field at iteration $n+1$ is determined by:

$$Q_{n+1} = \begin{cases} Q_0, & \text{if } (\delta_M + \delta'_n) > 0,\ \delta_M > 0 \\ Q_0 - \beta(\delta_M + \delta'_n), & \text{if } (\delta_M + \delta'_n) \leq 0,\ \delta_M > 0 \\ Q_0 + \beta(\delta_M), & \text{if } (\delta_M + \delta'_n) > 0,\ \delta_M \leq 0 \\ Q_0 - \beta(\delta'_n), & \text{if } (\delta_M + \delta'_n) \leq 0,\ \delta_M \leq 0 \end{cases} \tag{5.1.2}$$

Where δ_M is the mean (background) divergence and δ'_n is the anomalous divergence at iteration n, found by solving Equations 5.0.1 and calculating the divergence of the anomalous wind field. Q_0 is the initial, prescribed heating. Thus, if both the total field (background and anomalous) and the background wind field are divergent, then heating is only due to the diabatic term (as in the earlier model). If the background is divergent but the anomalous field is sufficient to make the total state convergent, then the heating is increased only in proportion to the net convergence of the field. If the background state is convergent but the anomalous field is sufficiently divergent to make the total field divergent, then the heating is reduced by a term proportional to the background convergence. Finally, if both the background field and the anomalous field are convergent, then the heating is enhanced in proportion to the anomalous field.

The solution for a specified fixed diabatic heating is found by an iterative procedure. Following Zebiak [1986], this moisture convergence feedback was incorporated into the atmosphere model of the current work, and results from the model were verified against those published by Zebiak. The calculated wind field for a simple sea surface temperature anomaly is shown in Figure 5, with a prescribed non-dimensional background divergence field having the following form:

$$\delta_M = \begin{cases} -6.0, & 0.5 < y < 1.5 \\ +2.0, & y < 0.5,\ y > 1.5 \end{cases} \tag{5.1.3}$$

This field roughly approximates the Intertropical Convergence Zone between 5°N and 15°N, with divergence to the north and south.

Though the initial diabatic heating is symmetric, the wind response is noticeably asymmetric with enhanced convergence of the anomalous wind field in the region with a specified background convergence. In this region, the original heating anomaly is magnified as both the anomalous and background wind fields are convergent. The overall effect of the moisture convergence term is to focus the atmospheric response of the model into regions of mean background convergence, in keeping with observations.

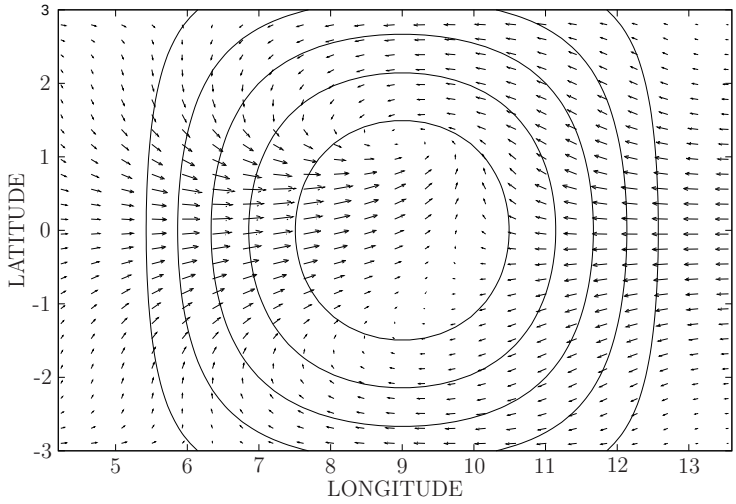

Figure 5: *Gill atmosphere response for heating parametrised by SST anomalies and background moisture convergence. The background state is prescribed to be convergent between* $y = 0.5$ *and* $y = 1.5$ *and divergent elsewhere. The SST anomaly is positive and contoured.*

As with the earlier, simpler model, Zebiak compared the response of this model including the moisture convergence term, to the observed atmospheric response to sea surface temperature anomalies. He found that the model was considerably improved in its off-equatorial response and that its large scale response to ENSO anomalies was now more realistic. As a results, it was this atmospheric model that was used in the subsequent development of the Zebiak-Cane model.

5.2 Incorporating a Gill model into GModel

Having successfully created the above model and verified its results against those published by Zebiak, it was incorporated into GModel, replacing the original statistical atmosphere model. A few modifications had to be made to the original code for GModel and the atmosphere model in order to properly implement it, and these are outlined below.

The original version of GModel did not include monthly climatologies of the sea surface temperature and wind fields, however these were required for the Gill atmosphere model both for calculating the heating parametrisation (the diabatic heating term requires the mean sea surface temperature to be known, and the latent heating term requires the background wind convergences to be known) and converting anomalous wind velocities to anomalous wind stresses. The "forced" mode of GModel used Florida State University observed wind pseudostresses decomposed into a zonal and meridional component over the time period 1966 to 1999, and it was this data that was used to create the monthly wind velocity climatologies required for the model. Given the definition of pseudostress:

$$\tau = |\mathbf{u}|\mathbf{u} \tag{5.2.1}$$

Velocity components the zonal and meridional directions were found using the relations:

$$\bar{u} = \frac{\tau_x}{(\tau_x^2 + \tau_y^2)^{\frac{1}{4}}} \tag{5.2.2a}$$

$$\bar{v} = \frac{\tau_y}{(\tau_x^2 + \tau_y^2)^{\frac{1}{4}}} \tag{5.2.2b}$$

The Florida State University data used was specified on a grid of resolution 30×84 gridpoints in the meridional and zonal directions respectively. In order to be used in GModel, the data was linearly interpolated onto a 61×86 grid.

Sea surface temperature anomalies were downloaded from the IRI/LDEO Climate Data Library from the ReynSmith dataset (R. W. Reynolds [1994]).

Once the background climatologies were established, the anomalous wind velocities calculated by the Gill model atmosphere could be converted into effective anomalous pseudostresses for forcing the ocean component. For the purposes of this work, it is convenient to define an effective pseudostress as:

$$\tau = \zeta|\mathbf{u}|\mathbf{u} \tag{5.2.3}$$

Where ζ is a dimensionless drag coefficient between the atmosphere and ocean, and hereafter τ is taken to mean an effective pseudostress. Velocity anomalies calculated by the model were converted to wind pseudostress anomalies using the relation that anomalous pseudostresses are simply the difference of the total pseudostress and the mean pseudostress at each gridpoint:

$$\tau'_{psx} = \zeta(|\bar{\mathbf{u}} + \mathbf{u}'|(\bar{u} + u') - |\bar{\mathbf{u}}|\bar{u}) \tag{5.2.4a}$$

$$\tau'_{psy} = \zeta(|\bar{\mathbf{u}} + \mathbf{u}'|(\bar{v} + v') - |\bar{\mathbf{u}}|\bar{v}) \tag{5.2.4b}$$

τ'_{psx} and τ'_{psy} are the anomalous effective wind pseudostresses in the zonal and meridional directions, $\bar{\mathbf{u}} = (\bar{u}, \bar{v})$ is the mean velocity, and $\mathbf{u}' = (u', v')$ is the anomalous velocity. A minor modification to the original code allowed it to keep track of the year and month so that the relevant climatology could be used at each timestep.

The inclusion of the moisture convergence term in the atmosphere model means that the model must iterate to (numerical) convergence at each timestep. The iterative variable is the "extra" heating term that accounts for latent heating by the atmosphere. At the beginning of the first timestep, this variable is completely unknown and the model takes many iterations to converge. However, the scheme adopted in this model (following Zebiak and Cane [1987]) is to carry over this variable between timesteps such that, provided there are no large changes in the sea surface temperature anomalies or background wind field, the number of iterations required for convergence of the model is reduced for subsequent timesteps. Due to the nonlinearity of the heating parametrisation, this scheme allows the development of unphysical small scale anomalies which are not related to the sea surface temperature. To prevent this, the iterative variable is set to zero every twenty days and recalculated from SST anomalies and the known background wind field at that timestep.

6 GModel + Gill: A standard run

Having fully incorporated the simple physical atmosphere of Section 5 into GModel, a 'standard run' of the coupled model was performed. The run was initialised by a westerly wind burst which was held constant over the first four months (from January to May) during which time the model was uncoupled. The imposed wind field had a Gaussian structure:

$$u_a = (0.2ms^{-1}) \exp\left[-\left(\frac{y}{20^\circ}\right)^2 - \left(\frac{(x-170^\circ E)}{25^\circ}\right)^2\right] \tag{6.0.5}$$

At the end of the fourth month the imposed wind field was removed, and replaced by the Gill model atmosphere. Parameters for the atmosphere model were kept as close as possible to the values used by Zebiak and Cane [1987], though some variation was necessary in order to obtain an ongoing oscillation as the ocean and SST parameters in GModel were different. A full list of the parameter values used is given in Appendix C. The impact of varying the parameters on the nature of the oscillation will be discussed in subsequent sections.

The average sea surface temperature anomalies in the regions 5°N - 5°S and 150°W - 90°W (the NINO 3 region) and 5°N - 5°S and 160°E - 150°W (the NINO 4 region) are plotted in Figure 6 for a 50 year 'standard' run. The SST shows clear ongoing oscillations during this time. The average period of the oscillation is 3.3 years with a maximum period of 3.7 years, and a minimum of 2.5 years. The maximum SST anomalies occur in the east with a peak amplitude obtained in the NINO 3 region of 1.8°C. The amplitude of positive anomalies tends to be somewhat larger than negative anomalies.

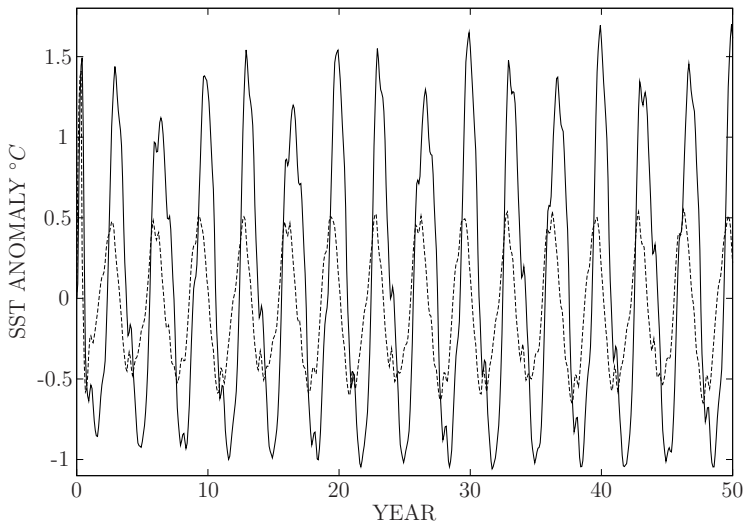

Figure 6: *SST anomaly in NINO 3 region (solid line) and NINO 4 region (dashed line) over 50 years for standard run.*

The oscillations are not entirely regular, and they show a prevalence for warm events to occur in the central to eastern Pacific primarily around either December but also

around June. SST anomalies peak in the NINO 4 region before the NINO 3 region, indicating that the warm or cool event tends to build in the central Pacific before propagating to the eastern boundary.

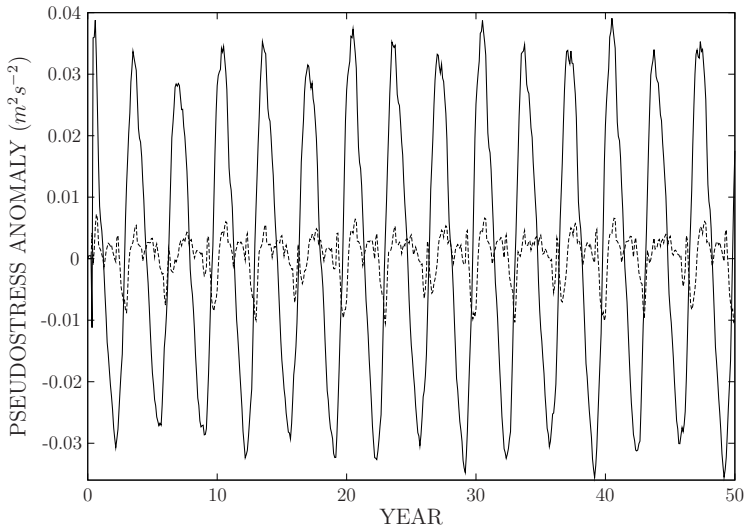

Figure 7: *Zonal (solid line) and meridional wind anomaly (dashed line) in NINO 3 region over 50 years for standard run.*

Spatially averaged wind anomalies over the NINO 3 region are shown in Figure 7. As with the SST anomalies, there is a clear oscillation in the zonal winds. An oscillation in the meridional winds is present, but has a much smaller amplitude and is subject to much more high frequency variability than the zonal winds. As both the NINO 3 region and the equations of motion governing the atmospheric response (Equations 5.0.1) are equatorially symmetric, the oscillation in the meridional wind stress must arise as a result of asymmetries in the equatorial heating or boundaries of the region. In particular peaks appear in the meridional wind stress indicating stronger northerly winds than southerly winds near the termination of a cool event.

The zonal wind stress anomalies lag the SST anomalies by approximately six months in the NINO 3 region, with peaks in westerly zonal wind stress occurring as the warm SSTs become more localised and intense along the eastern boundary. At first glance this may appear contradictory to observations which suggest that the peak of an El Niño event coincides with a general weakening of the Walker Circulation and strong anomalous westerly winds, however, the NINO 3 region under consideration is of large zonal extent and does not include the far eastern boundary of the basin. In this model, warm SSTs develop in the central Pacific and intensify whilst propagating to the eastern boundary, thus the actual peak of an El Niño event is several months later than the peak in the NINO 3 region, and coincides with the peak in westerly wind anomalies, in agreement with observation.

Screenshots of the SST anomaly field and wind anomaly vectors at different times during a typical oscillation are shown in Figure 8.

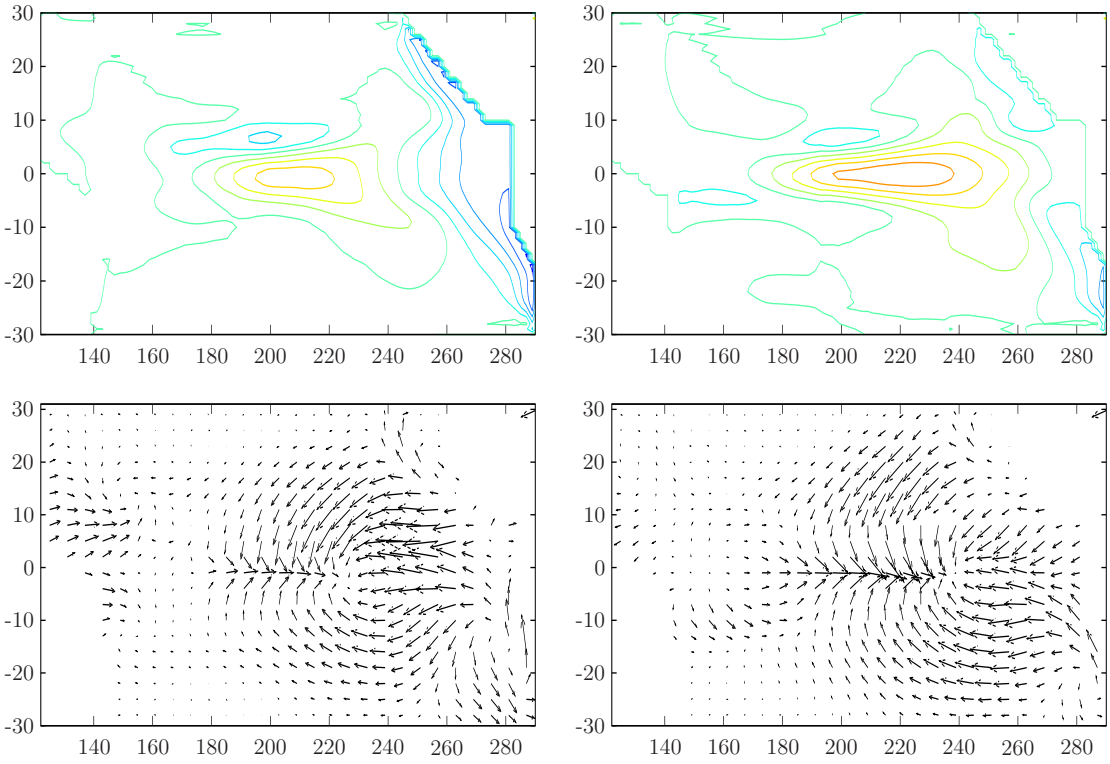

(a) *January year 9*

(b) *July year 9*

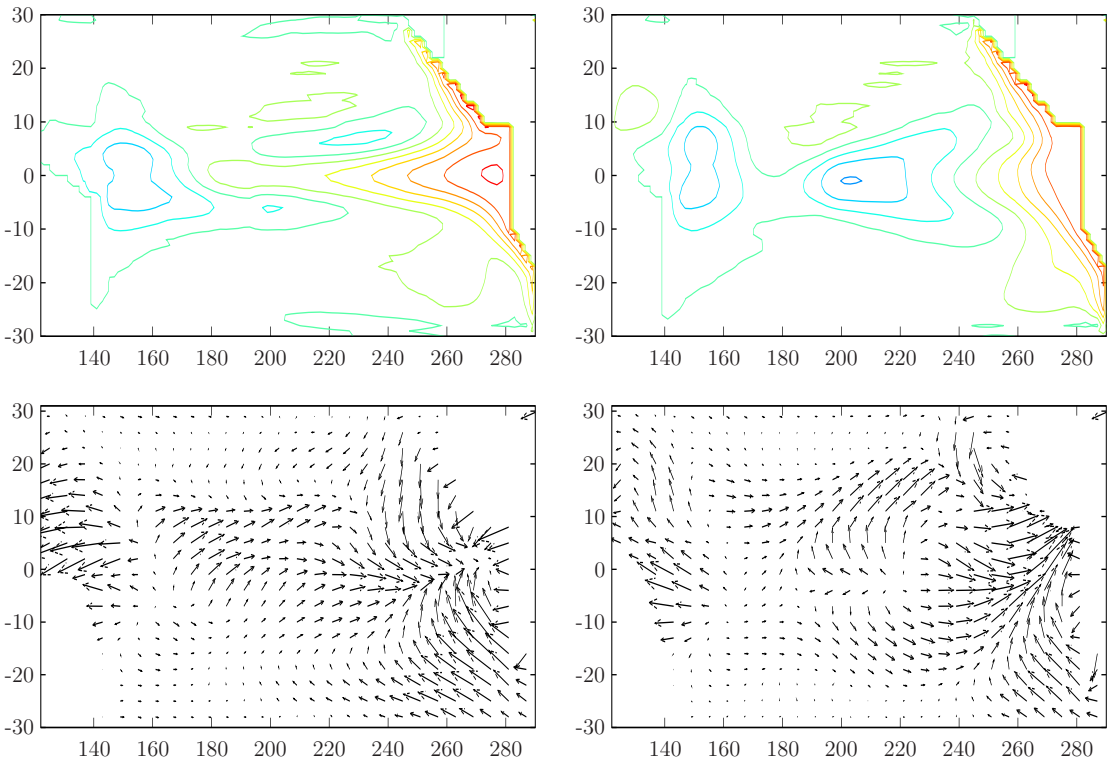

(c) *January year 10*

(d) *July year 10*

Figure 8: *Wind and SST anomaly fields during standard run (years 9 and 10). Temperature contours are every 0.5° C, with 0° C being turquoise.*

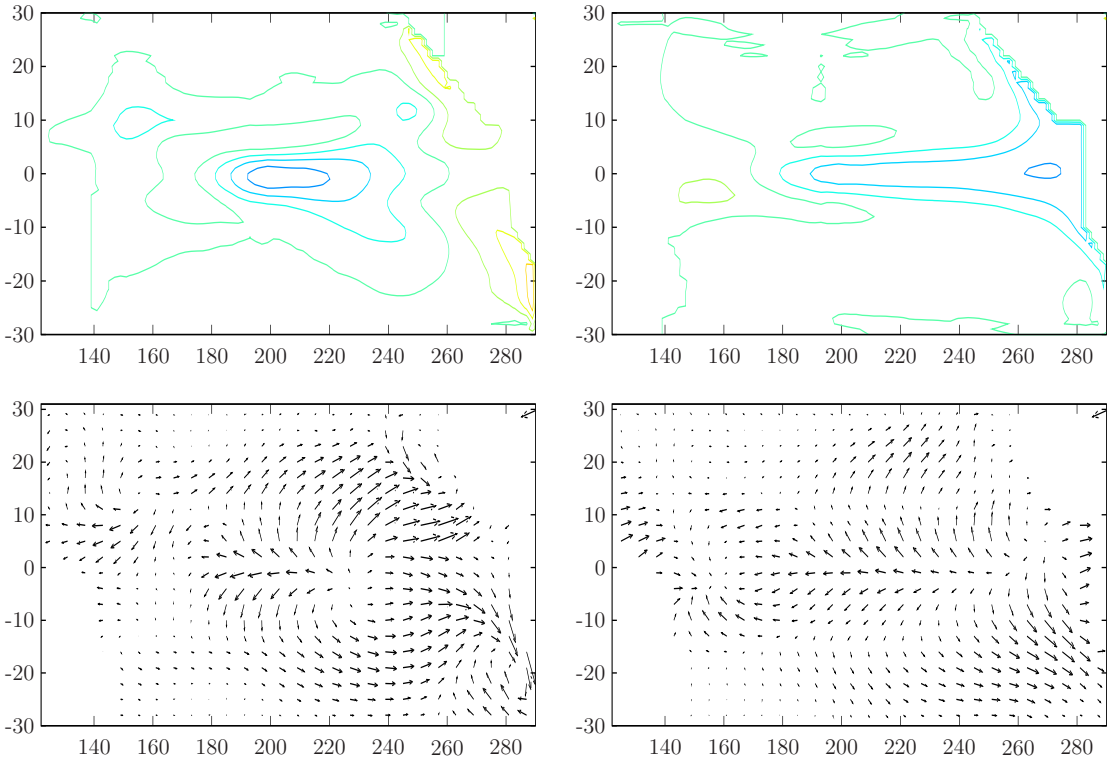

(e) *January year 11* (f) *July year 11*

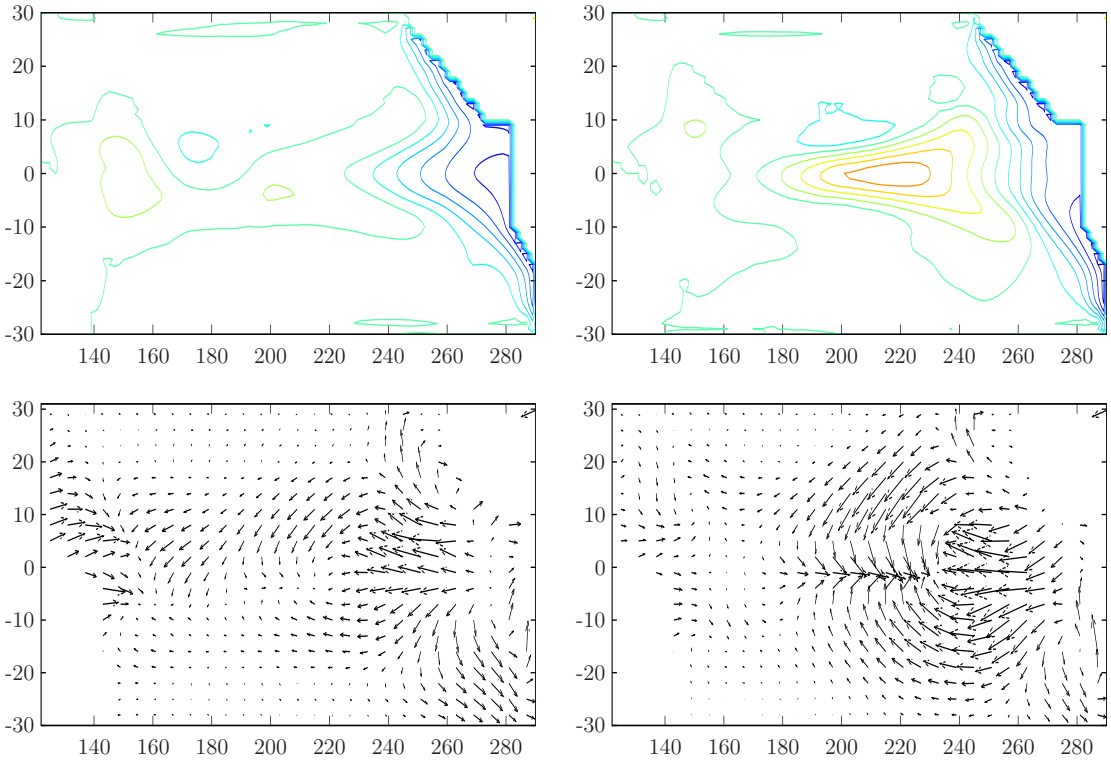

(g) *January year 12* (h) *July year 12*

Figure 8: *Wind and SST anomaly fields during standard run (years 11 and 12). Temperature contours are every 0.5° C, with 0° C being turquoise.*

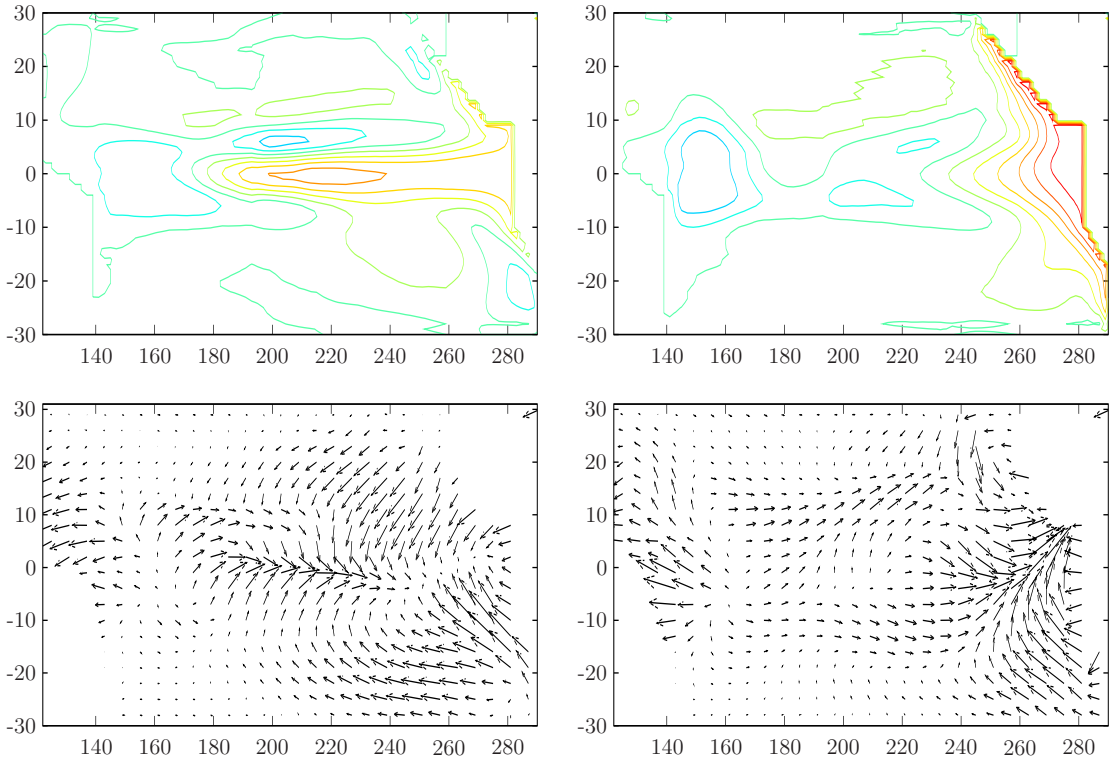

(i) *January year 13* (j) *July year 13*

Figure 8: *Wind and SST anomaly fields during during standard run (year 13). Temperature contours are every 0.5° C, with 0° C being turquoise.*

Figure 8(a) for January of year 9 shows the very end of a cool event and the beginning of the development of a warm event in the central Pacific. The warm sea surface temperature anomaly causes air to rise over the central Pacific, and westerly winds form to the west of the anomaly causing anomalous downwelling along the equator. This results in the destabilisation of downwelling (warm) Kelvin waves, and upwelling first order Rossby waves with peaks to the north and south of the equator (Hirst [1985]). The Kelvin waves grow and propagate eastwards taking with them the overlying westerly wind anomalies which, through positive feedbacks, cause the enhancement of the original anomalies. Simultaneously, upwelling Rossby waves propagate west along a deepened thermocline (where dissipative effects are relatively small) where they reflect off the western boundary and much of the wave energy is transformed into an upwelling Kelvin wave. By January of year 10, the signature of an El Niño event is strong in the eastern Pacific and westerly wind anomalies overly almost the entire basin causing the characteristic weakening of the Walker circulation. It is at this time that a peak in the zonal windstress anomalies is observed in Figure 7 as westerly wind anomalies overly the entire NINO 3 region, however, by this time the SST anomalies in the NINO 3 region are reduced compared to a few months earlier as the warmest SSTs have already propagated to the eastern boundary. This is the cause of the apparent phase lag between Figures 6 and 7.

Whilst the warm event strengthens and develops in the eastern Pacific, upwelling Kelvin waves propagate into the central Pacific where, once again, the positive feedback mechanism kicks in causing the growth of the cool anomalies and destabilising upwelling Kelvin waves and downwelling Rossby waves. The upwelling in the central Pacific gradually erodes away at the warm event in the east until in January of year 11, cool Kelvin waves propagate freely across the entire central to eastern Pacific with weak easterly winds overlying them. July of year 11 shows the typical features of a La Niña event with a general strengthening of the Trade winds, and cooler SSTs across the eastern portion of the basin.

By January of year 12, reflected warm Rossby waves generated during the formation of the current La Niña event begin to propagate to the central Pacific causing the cycle to begin again under the influence of positive feedbacks.

It is clear that the mechanism in this model is reliant upon the propagation of oceanic free modes, and positive feedbacks between the ocean and atmosphere which cause the enhancement of anomalies and the destabilisation of these modes. It was results such as this that inspired the development of the delayed oscillator model that has become the paradigm for ENSO oscillations (Suarez and Schopf [1988], Battisti and Hirst [1988]. In this mechanism, the current state of the coupled Pacific arises both as a result of processes ongoing at the time and ocean adjustment processes caused by events at a previous time. Modelling the system with a simple delay equation produces ongoing oscillations with similar large-scale characteristics to those observed in nature.

7 Gmodel + Gill: Model sensitivities

7.1 Parameters and coupling

The parameters used in the standard run are based upon those chosen by Burgers and Oldenborgh [2003] for Gmodel, and those used by Zebiak and Cane [1987] for the atmosphere model. However, in order to obtain an ongoing oscillation in the present coupled model it was necessary to make significant changes to some of the parameter values, in particular those relating to the heating parametrisation (α and β) and the drag coefficient relating wind velocity anomalies to wind stress anomalies (ζ). This is not entirely unexpected as the ocean model used by Zebiak and Cane [1987] is dynamically different to Gmodel and consequently the parameters responsible for indirect ocean-atmosphere couplings will be different for each model.

In order to understand the importance of different processes on the model oscillation, the impact of varying a few key parameters on the model oscillation is examined below. In each of the below experiments, all of the parameters other than that being varied are the same as for the standard run.

7.1.1 Thermal damping rate, γ_{sst}

The thermal damping rate is used in the SST equation (Section 4.2) and controls the damping of SST anomalies by heat loss to the atmosphere. The values used in the standard run were chosen by Burgers and Oldenborgh [2003] to best reproduce ENSO like oscillations in the ocean when forced by observed wind stress data, and they range from $(60\ days)^{-1}$ in the western Pacific, linearly increasing from 160°W to a maximum of $(14.77\ days)^{-1}$ in the eastern Pacific. Plots of the NINO 3 SST indices are shown in Figure 9 for two runs in which the rate in the eastern Pacific was first reduced by 3% compared to the standard run, then increased by 5% compared to the standard run. The values quoted in the captions are for the eastern boundary of the Pacific.

Decreasing the rate of thermal damping allows the ocean surface to hold heat for longer, thus SST anomalies are amplified. The amplitude of the oscillation is observed to increase, and the average period of the oscillation decreases to 3.1 *years* (compared to 3.3 *years* for the standard run). A striking feature of this run is an apparent low frequency oscillation in SST anomalies. Other runs (not shown) demonstrate that the period of the low frequency oscillation decreases with decreasing thermal dissipation rates.

Similarly, increasing the thermal damping rate results in greater heat loss by anomalies to the atmosphere, causing the maximum amplitude of the anomalies to be reduced. Figure 9(b) shows that the oscillation amplitude in this situation decays over time. The average period of the oscillation increases to 3.5 *years*.

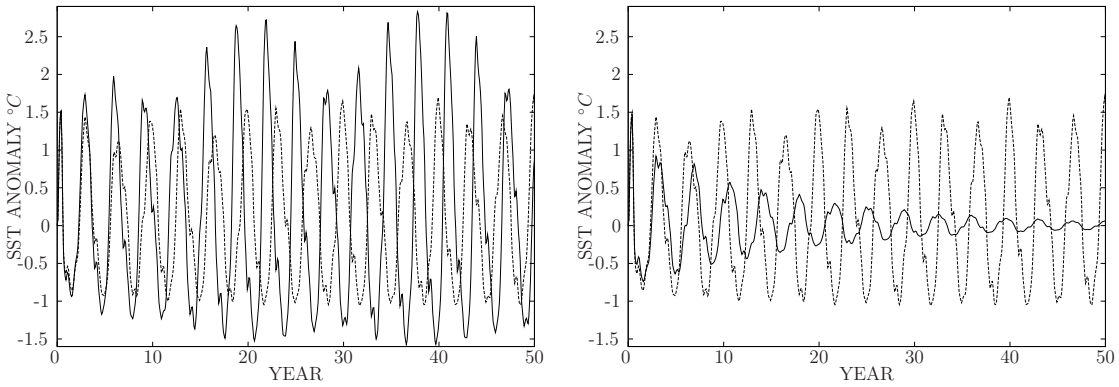

(a) *Thermal damping rate* $\approx$ *(15.15 days)*$^{-1}$. (b) *Thermal damping rate* $\approx$ *(14.21 days)*$^{-1}$.

Figure 9: *Comparison of standard run (dotted line) with test runs (solid line) where thermal damping rate, is a) decreased by 3% in the eastern Pacific, and b) increased by 5% in the eastern Pacific*

7.1.2 The equivalent depth, h_n

The equivalent depth, h_n, of a stratified fluid is the depth at which a homogeneous fluid layer having the same depth admits nth order Rossby wave solutions with the same propagation characteristics as those in the stratified fluid (see Appendix A). As such, changing the equivalent depth of the model changes the propagation characteristics of the free mode solutions in the ocean. The Kelvin wave speed for an equivalent depth, h_n, is given by $c = \sqrt{gh_n} = \sqrt{g'H}$, where g' and H are the reduced gravity and depth of the shallow water layer respectively. For these runs the equivalent depth was varied by changing both the Kelvin wave speed parameter and the depth of the shallow water layer such that the reduced gravity was kept constant.

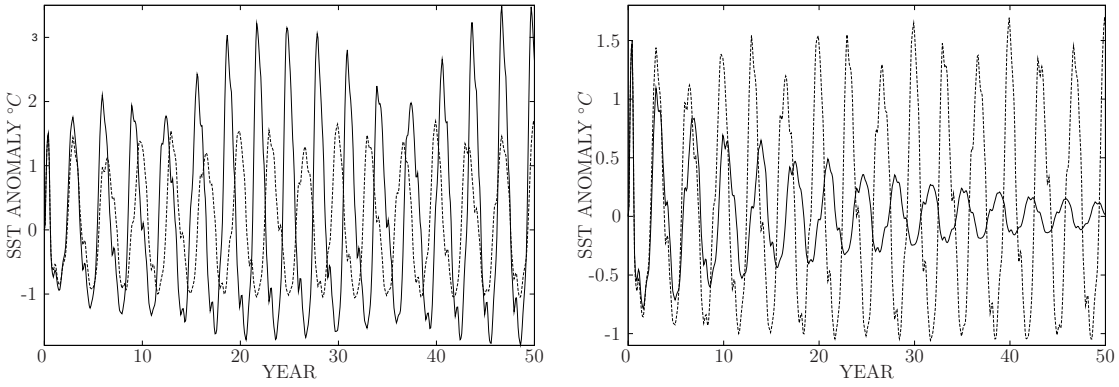

(a) *Equivalent depth reduced by 2%* (b) *Equivalent depth increased by 2%*

Figure 10: *Comparison of standard run (dotted line) with test runs (solid line) where equivalent depth is varied from standard run by 2%*

The amplitude of the oscillation depends sensitively on the equivalent depth, with shallower depths causing the oscillation amplitude to increase and period to decrease.

The change in amplitude of the oscillation can be understood by consideration of the depth integrated horizontal momentum equations for the shallow water layer:

$$\frac{d(Hu_1)}{dt} - \beta_0 yHv + g'H\frac{\partial \eta_1}{\partial x} = \tau_x - F_M(uH) \tag{7.1.1a}$$

$$\frac{d(Hv_1)}{dt} + \beta_0 yHu + g'H\frac{\partial \eta_1}{\partial y} = \tau_y - F_M(vH) \tag{7.1.1b}$$

The only terms that are not scaled by the depth of the shallow water layer are the windstress terms, thus a reduction of the depth of the shallow water layer (or equivalent depth) is equivalent to increasing the windstress in these equations. As such, larger currents are generated and the thermocline depth anomaly is greater per unit windstress. A larger thermocline anomaly causes larger SST anomalies, which in turn generate larger wind stresses. This positive feedback loop between the ocean and atmosphere ultimately causes the oscillation amplitude to increase. A similar argument holds for the reduction in amplitude observed when the equivalent depth is increased.

It is interesting that this result contradicts the result that would be expected from a pure delayed oscillator mechanism. In the case of a delayed oscillator, increasing the Kelvin wave speed would cause the period of the oscillation to increase due to the longer time taken by Kelvin and Rossby waves to cross the Pacific. Evidently in this model, the effects of changing the coupling dominate the behaviour of the oscillation.

7.1.3 Drag coefficient between windstress and ocean, ζ

This coupling parameter directly affects the strength of the oceanic forcing per unit wind velocity and is a factor in the wind pseudostress equations, 5.2.

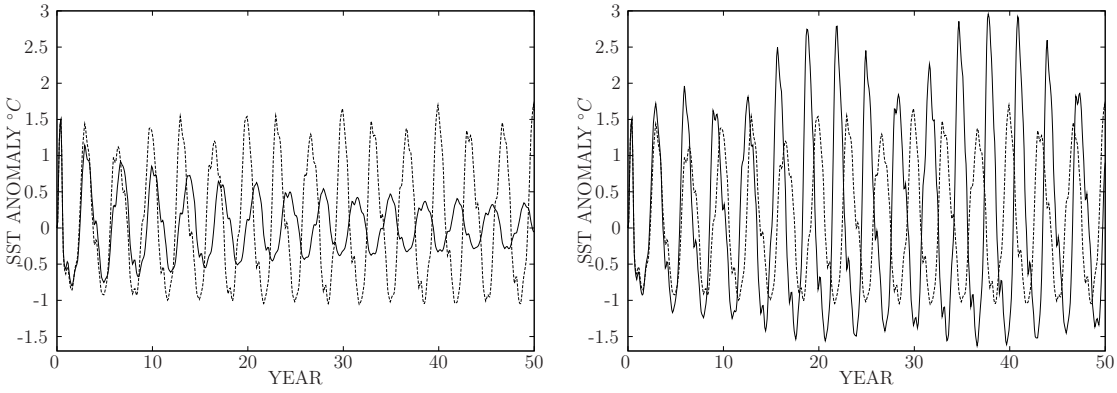

(a) *Drag coefficient reduced by 2%* (b) *Drag coefficient increased by 2%*

Figure 11: *Comparison of standard run (dotted line) with test runs (solid line) where drag coefficient is a) reduced by 2% and b) increased by 2%*

Reduction of the drag coefficient causes the amplitude of the oscillation to decrease with each period, while the period of oscillation is increased (3.5 *years*). Increasing the drag coefficient has the opposite effect, causing the amplitude of the oscillation to increase and shorten its period to around 3.1 *years*.

The oscillation is sensitive to variations in the size of the drag coefficient with variations of more than about 2% causing the oscillation to either rapidly increase in amplitude causing the run to terminate, or become rapidly damped. The sensitivity arises due to a positive feedback whereby increased effective wind stress drives stronger currents in the ocean, causing larger SST anomalies which in turn force larger wind anomalies.

7.1.4 Heating coefficients, α and β

The diabatic and latent heating terms govern the amount by which a given temperature anomaly, and given wind convergence respectively will contribute to atmospheric heating and thus the forcing of wind anomalies.

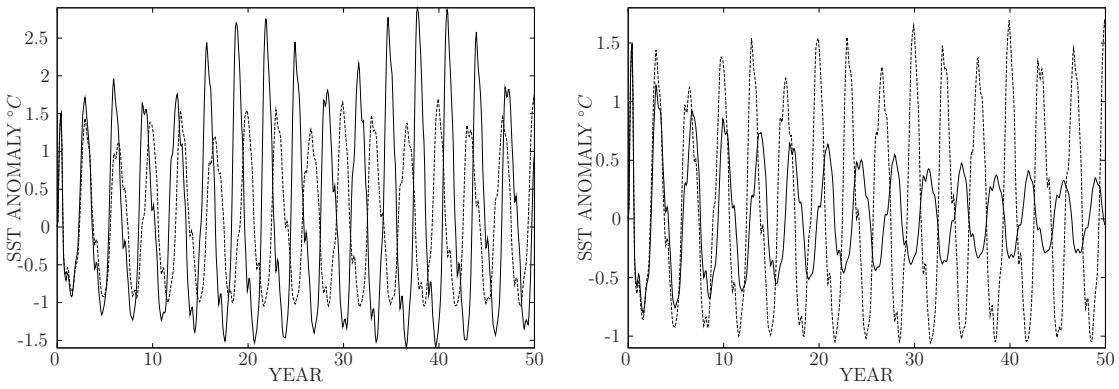

(a) *Diabatic heating factor increased by 2%* (b) *Diabatic heating factor decreased by 2%*

Figure 12: *Comparison of standard run (dotted line) with test runs (solid line) where diabatic heating factor, α is a) increased by 2% and b) reduced by 2%*

The oscillation amplitude is sensitive to changes in the diabatic heating parameter which directly affects the coupling of the model. Changes in the characteristics of the oscillation are indistinguishable to those observed to arise from small changes in the drag coefficient. However, changes in the latent heating parameter have significantly less effect on the model oscillation indicating that moisture convergence feedback has less influence on the large scale features of the oscillation than direct diabatic heating.

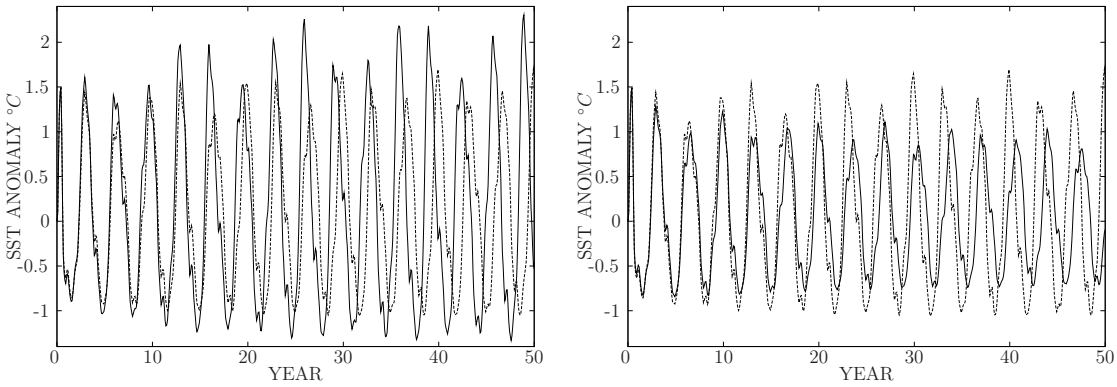

(a) *Latent heating factor increased by 5%* (b) *Latent heating factor decreased by 5%*

Figure 13: *Comparison of standard run (dotted line) with test runs (solid line) where latent heating factor, β is a) increased by 5% and b) reduced by 5%*

7.1.5 General features arising from changed coupling

All of the above parameter changes have resulted in either an indirect or direct change in the coupling of the model, causing the amplitude and period of the oscillation to change. It is notable that the overall features of an oscillation with increased/decreased coupling are the same, regardless of the parameter change that caused the increase/decrease in coupling. In general, increases in coupling cause the amplitude of the oscillation to increase and the period to decrease with a low frequency oscillation appearing in the amplitude. Parameter changes causing the coupling to decrease result in a damped amplitude with an oscillation that dies away over time. The period of such oscillations is longer, and itself exhibits a sizeable oscillation (for example in the case of wind drag reduced by 2%, the period oscillates between $37 months$ and $47 months$).

A striking feature of the more strongly coupled experiments is the presence of an overlying low frequency oscillation. This interdecadal variation is more prominent in the amplitude of warm events than cold events due to the increased propensity for the growth of warm anomalies than cool in the Pacific, and it arises through the interaction of the seasonal cycle with the shortened period of oscillation associated with increased coupling. The runs in this section have been initialised in the same manner: an imposed westerly wind burst in the central Pacific is held constant for four months whilst the model is uncoupled. Downwelling Kelvin waves are destabilised and propagate freely to the eastern boundary. After four months, the initialising wind field is switched off and the Gill atmosphere takes over, responding in an approximately physical manner to the sea surface temperature anomalies and allowing positive feedback mechanisms between the ocean and atmosphere to arise. Upwelling Rossby waves destabilised by the imposed initial wind field reflect from the western boundary, and as the Gill atmosphere starts, reflected upwelling Kelvin waves begin to propagate into the central Pacific where positive feedbacks cause them to grow. In runs where a changed parameter has caused the coupling of the

model to increase, the growth rate is faster and the cool sea surface temperature anomalies in the central Pacific rapidly reach a sufficient size to negate the warm event at the eastern boundary caused by the initial imposed winds. This mechanism is more pronounced for larger amplitude oscillations as larger anomalies are subject to larger feedbacks causing them to have larger growth rates than smaller anomalies. The finite time required for Kelvin waves to propagate across the central Pacific and reflect off the east coast causes the amplitude of the oscillation to increase as even once the incoming event has taken hold in the eastern Pacific, it continues to grow under the influence of feedbacks. As such, there is the potential for successive events to be of larger and larger amplitude, and this is observed when the coupling of the model is increased above a threshold amount (not shown).

Gradually, the effects of a stronger coupling on the period causes the oscillation to move out of phase compared to an oscillation with standard coupling and it is the interaction of this effect with the seasonal cycle that causes the low frequency variability in the overlying oscillation. Present in all oscillations with the seasonal cycle progressing in the background, is an annual 'notch' in the Nino 3 index. In the standard run, the peak of warm events tends to coincide with the notch which occurs under November and December background conditions, thus it is only really visible in alternate years. However, in the runs with changed coupling and changed period, the notch is more prominent and provides a convenient way of observing the progression of the phase of the oscillation through the annual cycle. In particular, warm events tend to reach a maximum amplitude where November/December conditions occur just before the peak of the cool event. It is whilst the La Niña event is in full swing in the eastern Pacific that warm anomalies begin to grow in the central Pacific, so this result indicates that anomalies which begin their growth period in the central Pacific during the boreal spring are subject to increased coupling over the duration of their growth period causing the final amplitudes of their oscillation to be larger than those that are initiated at other times of the year. The effects of the seasonal changes in background conditions will be considered in more detail in the next section.

7.2 Seasonal effects

As noted in Section 6, the model shows a tendency for warm events to reach their peak either near the end of the year or in the middle of the year. This eventually occurs irrespective of the starting month of the run indicating that the oscillation is phase locked with the annual cycle.

Running the model with the background sea surface temperature and wind field held fixed (i.e. no seasonal progression) gives markedly different results depending upon the month chosen for the background state. Background conditions fixed in December, January, February, July or August result in oscillations with steadily increasing amplitudes causing the eventual early termination of the run. Conditions fixed in all other months either result in steady ongoing oscillations, or slowly

damped oscillations whose amplitudes reduce over time. The least favourable background conditions for the oscillation are those that occur in April and May, where the maximum amplitude of SST anomaly attained is around 0.2° and the amplitude of oscillation reduces thereafter. Clearly, the seasons affect the coupling of the ocean atmosphere system and at some times of the year the background state is more conducive to positive feedbacks between the ocean and atmosphere than at others.

In order to investigate this effect more thoroughly, a 'typical' oscillation was chosen from the standard run, and the seasonal progression was switched off at different times during the development of the oscillation.

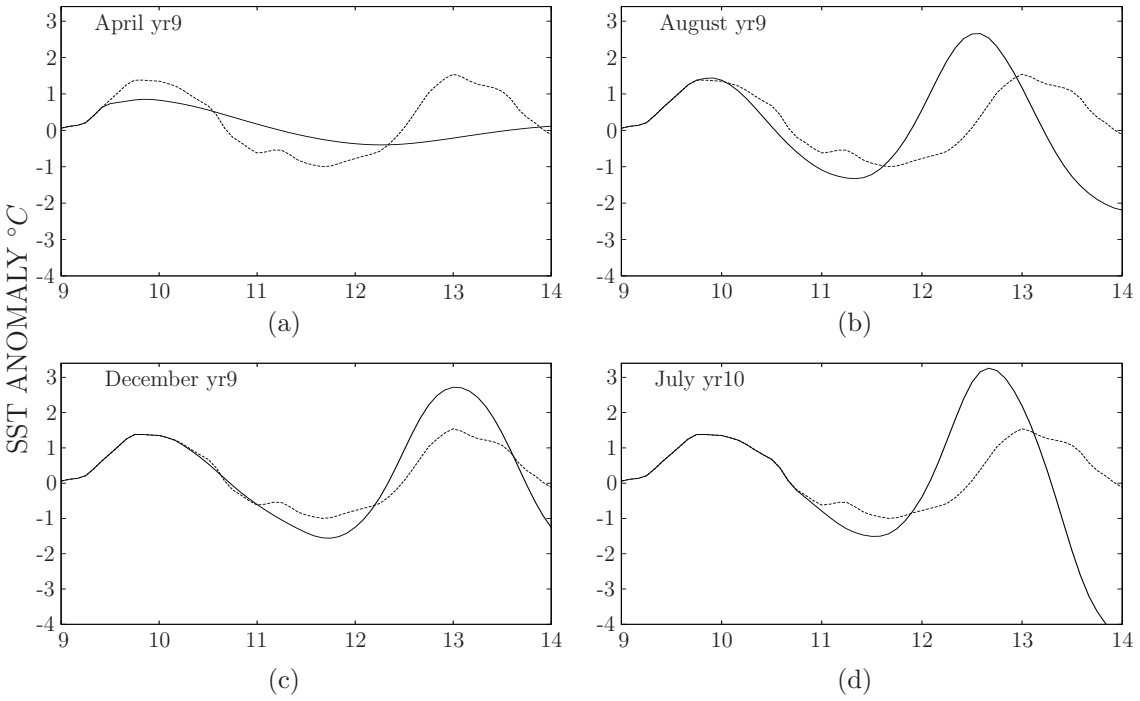

Figure 14: *Comparison of standard run (dotted line) with test runs (solid line) where progression of seasons is stopped at a) April conditions, b) August conditions, c) December conditions and d) July conditions. The time is shown in years along the y-axis.*

Figure 14 shows the effect of holding the seasons fixed compared to allowing them to progress as in the standard run. Of the four months investigated, only April conditions cause the oscillation to be damped. The period of the oscillation is slightly longer, and the amplitude of the developing warm event is reduced by around 0.5° compared to the standard run. August, December and July conditions all cause the subsequent oscillation to increase in amplitude and have a reduced period.

The growth of SST anomalies to larger amplitudes during some seasons suggests that the coupling strength between the ocean and atmosphere is modulated by the background climatology. In this model the background climatologies are used as follows: the mean SSTs are used in calculating the diabatic heating anomaly term, and the mean winds are used in calculating the latent heating anomaly term and

the anomalous pseudostress terms. The diabatic heating term takes the following form:

$$Q_0 = \alpha \Delta T \exp[(\bar{T} - 31°C)/17.3°C] \tag{7.2.1}$$

Thus, heating is more effective against a warm background sea surface temperature. The latent heating term is given in Section 5.1 and causes heating to be enhanced in regions of overall atmospheric convergence. The anomalous pseudostress is calculated by Equations 5.2 which cause anomalous pseudostresses to be larger where the background winds are stronger. Contour plots of the background climatologies are given in Appendices E to G and show that there is considerable variation in both the wind fields and sea surface temperature fields throughout the year. Of most importance to ENSO is the region in the central to eastern Pacific where anomalies develop and propagate. Monthly spatial averages between 10°N - 10°S and 160° - 220°E (central Pacific) and 220° - 280°E (eastern Pacific) are plotted in Figure 15. Values have been normalised by the maximum value attained across both regions for each of the variables being measured.

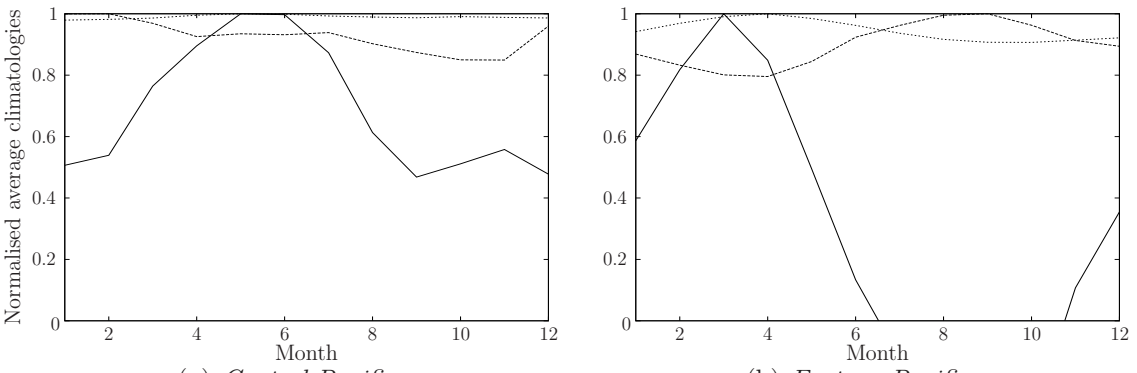

(a) *Central Pacific* (b) *Eastern Pacific*

Figure 15: *Normalised averages of wind convergences (solid line), wind speeds (dashed line) and SSTs (dotted line) in eastern and central Pacific*

The convergence of the mean wind field undergoes the most dramatic seasonal variation in the eastern Pacific, peaking in spring when the Inter Tropical Convergence Zone (ITCZ) extends southwards towards the equator. Between July and November, the wind field in the eastern Pacific is divergent as the ITCZ moves north of the equator. Roughly in phase with the wind convergences is the SST which also peaks early in the year though exhibits a far smaller percentage variation of around 10% in the eastern Pacific, and 1-2% in the central Pacific. The mean wind speeds in both regions vary by around 20%, having a minimum in the eastern Pacific during the boreal spring when the Trade winds are at their weakest.

Variations in the background conditions are equivalent to variations in the model parameters at fixed background conditions. Accordingly, a decrease in the background wind speed is equivalent to a decrease in the drag coefficient, ζ, at fixed wind speeds. Changes to the background convergence are largely equivalent to changes to the latent heating parameter, β, at fixed convergence (neglecting anomalous convergences), and changes to the background sea surface temperatures are equivalent

to changing the diabatic heating parameter, α. This means that the results of the sensitivity studies of Section 7.1 may be used to interpret the the results of changing the seasonal progression in the model.

Given the quadratic nature of Equation 5.2, a change of 20% in the background wind speed causes a change of around 45% in the anomalous wind stress for a given wind speed anomaly. This is equivalent to changing the drag coefficient relating the wind velocities to effective wind stresses by the same percentage. The sensitivity studies of Section 7.1.3 demonstrate that the model coupling is more sensitive to this parameter than to either of the parameters governing the latent and diabatic heating in the model. As such, it is unsurprising that anomaly growth in the eastern Pacific is stunted when background conditions are fixed in April and the wind speeds in the eastern Pacific are at their minimum. This occurs despite the maximal values of both the SST and wind field convergence in the eastern and central Pacific at this time, demonstrating that the growth rate of anomalies (coupling) in this model is dominated by the background wind speeds rather than factors affecting the heating rate of the atmosphere.

This results arises as the wind stress anomaly term appears not only as a forcing in the ocean model, but also as a term in the SST anomaly equation. Consequently the effects of reducing its magnitude are twofold as both the thermocline perturbation and the SST anomaly arising from zonal currents per unit wind anomaly are reduced. The net result is that both amplifying terms in the SST equation (Equation 4.2.1) are diminished, causing the overall temperature anomaly to be reduced. Though the latent and diabatic heating terms are maximal at this time, they are acting on small temperature anomalies thus the overall heating in the model is still reduced.

In the standard run, the model shows a disposition for seasonal locking with warm events tending to peak around the end of the year. Figure 15(b) shows that the wind speeds in the eastern Pacific are maximal in September causing the model to be strongly coupled in this region at this time. As a result, the growth rate of anomalies in the eastern Pacific during the second half of the year would be larger than earlier in the year, with a transition between the two regimes occurring at the very end of the year. The development of warm events in the standard run is initialised in the central Pacific where Rossby waves reflected from the western boundary as Kelvin waves accumulate and grow. This has a tendency to occur during the boreal spring, as it is during this time that Figure 15(a) shows maximal convergence with median wind speeds in the central Pacific region. Also at this time the coupling in the eastern Pacific is at its weakest, allowing the event in the east to be more efficiently eroded away by the developing event in the central Pacific. By September the anomalies in the central Pacific have grown, propagating east and eroding the previous event which has suffered less favourable growth conditions through the middle of the year. Background conditions in the eastern Pacific become favourable for continued anomaly growth and the new event takes hold, reaching its peak amplitude around the end of the year, or beginning of the next year. Conditions in January and February cause the growth rate in the eastern Pacific to drop, and as the Trade winds reach their annual minimum in spring the cycle begins again.

This time though, the anomalies are of opposite sign causing the alternate phase of ENSO to dominate the eastern Pacific. It is this balance of conditions across the central and eastern regions of the Pacific ocean throughout the year that cause the ENSO cycle to be seasonally locked with a period of approximately three years.

These conclusions support the results of Section 7.1.5 in which it was observed that by changing the coupling of the model itself and thus forcing a changed period of oscillation, anomaly growth periods initiated during the boreal spring resulted in larger warm events than when the warm anomaly growth period occurred at other times of year. These anomalies are subject to favourable growth conditions in the central Pacific before they propagate to the eastern Pacific where, by the end of the year, strong background winds cause the amplification of anomalies to form full El Niño and La Niña events. Evidently the tendency of the oscillation to be seasonally locked in this model is sensitive to the overall coupling, however, under conditions where the coupling is sufficient to give ongoing, steady oscillations that are neither growing or decaying over time, the timing of the development of anomalies in the central Pacific to full scale events in the east is affected by the seasonal cycle. With larger or smaller couplings, the seasonal cycle no longer governs the timing of the oscillation.

7.3 Model initialisation

Previous sections suggest that the period of the oscillation is determined by the coupling, which alters the growth rate of anomalies in the central Pacific and thus the time required for an incoming event to overcome the current event in the eastern Pacific. To clarify this mechanism, three further runs were done in which the duration of the initialising wind stress was reduced and the coupling varied.

In each of the following runs, the initialising wind stress was held constant for only two months (compared to four months in the standard run). As a result, the amplitude of subsequent oscillations is less. In the first run, all other parameters are exactly the same as in the standard run, whilst in the second and third the drag coefficient between the ocean and atmosphere is first increased by 2% then decreased by 2% causing an increase and decreased in model coupling respectively.

In the run using standard parameters, the period of the oscillation is unchanged, though the reduced initial conditions have caused the amplitude of the oscillation to be considerably smaller. Changing the coupling appears to have similar effects irrespective of the magnitude of the initial condition. This demonstrates that the period of the oscillation is set by the coupling of the model, not by its amplitude. Consequently, the growth rate of anomalies having a smaller amplitude must be correspondingly less indicating that for fixed coupling, the growth rate is set by the amplitude of the anomalies. These results suggest that the development of anomalies in the eastern Pacific may be considered, to first order, by analogy to a simple harmonic oscillator such as a pendulum. This idea will be considered more fully in the next section.

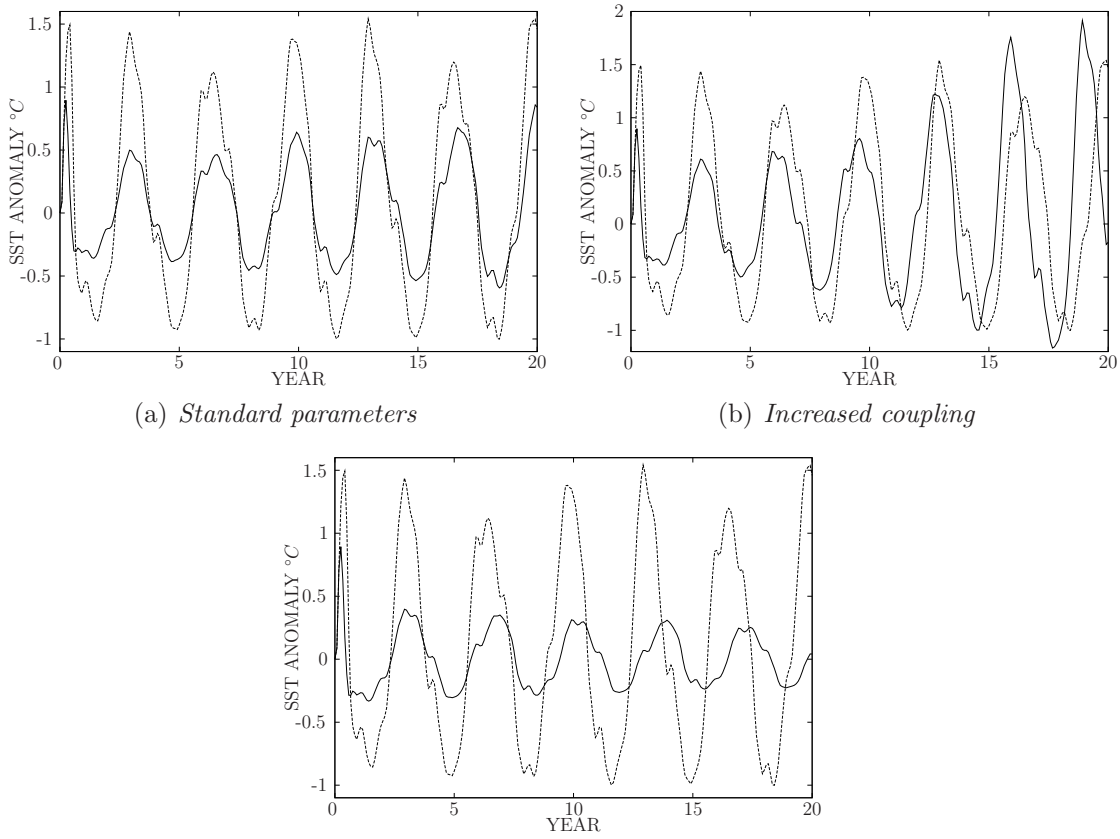

(a) *Standard parameters*

(b) *Increased coupling*

(c) *Reduced coupling*

Figure 16: *Comparison of standard run (dotted line) with test runs (solid line) where duration of initialising wind stress is halved compared to the standard run. In a) parameters are set as for standard run, b) drag coefficient ζ is increased by 2% and c) drag coefficient reduced by 2%*

8 The ocean, pendulums and delayed oscillators

Results of previous sections suggest that the sea surface temperature in the eastern Pacific oscillates with characteristics that are very similar to those of a simple harmonic oscillator, such as a pendulum. Briefly, the equations describing the simple harmonic motion of such a pendulum are given below:

$$x = A\cos(\omega t + \phi) \tag{8.0.1a}$$

$$v = -A\omega\sin(\omega t + \phi) \tag{8.0.1b}$$

$$T = \frac{2\pi}{\omega} = 2\pi\sqrt{\frac{l}{g}} \tag{8.0.1c}$$

$$E = \frac{g}{2l}A^2 \tag{8.0.1d}$$

x, v and a are the displacement, velocity and acceleration, ω is the frequency, T the period, l is the length of the pendulum, g the gravitational acceleration, A is the amplitude of the oscillation and E is the total energy. By analogy for this model the displacement x becomes the sea surface temperature anomaly in the eastern Pacific, with v being its growth rate. $\sqrt{l/g}$ are physical parameters of the oscillator, and for this system may be considered to be a 'coupling coefficient' describing the amount by which the system is coupled. Thus, in the same way that the natural frequency of a pendulum is governed by its length and mass, the natural frequency of the coupled ocean-atmosphere is governed by its coupling. Similarly gravity, the restoring force on a pendulum, becomes in analogy the subsurface memory component of the coupled system. The maximum growth rate of the system is described by a function depending upon both the coupling and the amplitude:

$$v_{max} = A\sqrt{\frac{g}{l}} \tag{8.0.2}$$

Therefore, at constant coupling the growth rate depends only upon the amplitude of the oscillation (which itself is determined by the initial conditions), in keeping with results from Section 7.3. Finally, the energy of the system is a constant, and is determined by the coupling and amplitude of the oscillation.

However, in cases where the coupling is above or below the values used in the standard run, the amplitude of the oscillation is observed to grow or decay with time. As such, the energy of the system is no longer constant and changes with the amplitude, which itself is a function of the coupling coefficient and time. The linear harmonic oscillator analogy breaks down in these cases and a non-linear oscillator is more appropriate.

Such a non-linear delayed oscillator model was considered by Battisti and Hirst [1988] (BH), and it may be simply described by the below equation:

$$\frac{\partial T}{\partial t} = -bT(t-\tau) + cT - e[T - rT(t-\tau)]^3 \tag{8.0.3}$$

In this model, T is the temperature anomaly in the eastern Pacific, t is the time, τ is related to the time taken by Kelvin and Rossby waves to traverse the Pacific basin and the coefficients b, c, e and r describe the relative importance of different physical processes to the oscillation. Neglecting non-linearities and differentiating the above equation with respect to time, an equation describing simple harmonic motion is obtained. The mechanism of this model may be easily understood and fits the results found in earlier sections. In essence it relies upon the destabilisation of Kelvin and Rossby waves by anomalous wind stresses in the central Pacific. These waves propagate to the east and west respectively, carrying with them an associated temperature anomaly caused by upwelling or downwelling within the wave. Kelvin waves formed by the reflection of Rossby waves at the western boundary are responsible for the switching of the oscillation from one phase to the other by providing the system with a 'memory' so that delayed effects can influence the oscillation. BH demonstrate that the period of their 'delayed oscillator' model is set by both the Kelvin wave speed, and the time taken for anomalies growing in the central Pacific to overcome the event in place in the eastern Pacific. Non-linearities in the model were found to be crucial in obtaining stable non-growing or decaying amplitudes.

Results from Section 6 suggest such that a delayed oscillator mechanism is likely to be largely responsible for the observed model oscillations. It would be interesting to more thorougly explore the similarities between the analytic delayed oscillator equation stated above, and the oscillation observed in this model. It is plausible that the model used in this work is a close linear analogy to the delayed oscillator mechanism discussed by BH (see Equation 8.0.3) as it contains no mechanism to prevent the unbounded growth of the oscillation. BH showed that their linear delayed oscillator was extremely unstable to changes in coupling which caused its amplitude to exhibit ongoing unbounded growth for moderate couplings. A systematic examination of the parameters used in this model from a dynamical systems perspective, similar to that performed by BH, might also yield more general results relating the model amplitude, period and coupling.

Unfortunately the delayed oscillator model, though persuasive in its simplicity, does not account for all of the observed features of ENSO. Often, observed SST anomalies appear in the central to eastern Pacific and show little sign of propagation, indicating that they are not simple Kelvin waves. Neelin [1990] proposed an alternate mode of the coupled ocean-atmosphere system in which the ocean was in quasi-steady balance with the anomalous wind stresses. In order to understand the mechanism of this slow SST mode, it is instructive to consider the limit whereby the ocean quickly adjusts to surface wind stresses, the so-called "fast-wave limit". In this case, a patch of warm SST causes a convergent wind field above it, with westerly winds located to the west of the SST. Ekman transports associated with the westerly wind anomalies cause downwelling located to the west of the original warm SST. Simultaneously, easterly winds to the east of the warm anomaly cause upwelling. The net result is that downwelling spreads to the west of the warm anomaly, and upwelling impinges at the east, causing the warm anomaly to propagate slowly westwards. However, a competing process occurs with thermocline feedbacks wherein westerly anomalies to

the west of the warm SST cause the thermocline to deepen in the east and creating eastward propagating tendencies (easterly anomalies to the east of the SST anomaly have little effect due to the background zonal tilt in the thermocline). Depending upon the relative strengths of the Ekman and thermocline feedbacks, the result will be a succession of slow moving warm and cool anomalies.

Of particular importance to ENSO however is the case of a slow SST mode in the eastern basin. In this case, a warm anomaly in the eastern Pacific gives rise to westerly wind anomalies to the west, causing downwelling to the west of the warm anomaly. The easterly wind anomalies to the east of the warm SST overly land, thus there is no upwelling to the east of the warm anomaly and the original warm anomaly is stationary. Instead, the combined response of the thermocline and Ekman currents cause the anomaly to spread westwards and intensify in a standing oscillation.

Jin and Neelin, in a series of publications in 1993, suggested that a more realistic mechanism for ENSO consisted of a mixture of slow SST and ocean dynamics modes. In this case, stationary SST modes grow in the eastern Pacific under the influence of ocean-atmosphere coupling, whilst free Kelvin and Rossby waves form the memory of the system, carrying it from one phase of the oscillation to the next.

9 Conclusion

Using a reliable and well tested 1.5 layer, linear ocean and sea surface temperature anomaly model as a foundation, an intermediate complexity model was created by coupling a simple Gill type atmosphere to the ocean model. The heating parameterisations in the Gill model and the requirement of coupling the calculated wind velocities to the ocean necessitated the introduction of a monthly climatology to define the 'background state' of the Pacific in terms of the wind fields and sea surface temperatures.

The coupled model was initialised by an imposed wind stress forcing which was switched off after a specified period, and replaced by the Gill atmosphere. The subsequent evolution of the model displayed ongoing oscillations in sea surface temperature and zonal wind anomalies over the eastern and central Pacific regions. A 'standard run' was defined to be one where the set parameters caused the oscillation amplitude to neither grow or decay over a 50 *year* run. The standard oscillation exhibited some of the features and irregularities associated with ENSO in nature in both its amplitude, period and tendency to become phase locked with the annual cycle.

A series of experiments changing the values of various parameters within the model were found to have strikingly similar outcomes in the nature of the model oscillation. Changes to these parameters all ultimately caused the coupling of the model to decrease or increase (with varying sensitivity) and it was this change that dominated the behaviour of the resulting oscillation. A further series of experiments involved fixing the progression of the seasonal cycle at different stages of a standard oscillation. The subsequent evolution of the oscillation was strongly affected by changes to the seasonal cycle, demonstrating that the coupling of the ocean-atmosphere system is significantly modified by the seasons. By examining the changes in the climatologies in the central and eastern Pacific over the duration of a year, and keeping in mind the results of the earlier parameter sensitivity studies it was shown that the seasonal coupling is most strongly dominated by fluctuations in the background wind speeds, and that it is the balance of climatologies in the central and eastern Pacific throughout the year that cause the model oscillation to become seasonally locked.

Finally, it was demonstrated that in cases of no amplitude growth or decay, the model oscillation appears to behave as a simple harmonic oscillator with a resonant frequency set by the physical parameters of the system. A non-linear mechanism of mixed slow SST modes and ocean dynamics was suggested as a more general dynamical model.

To fully understand the mechanism of the model oscillation, and relate it to ENSO in nature, further investigation of the parameters and the relative importance of their associated processes would be required. Dynamical systems theory has been successfully used by authors such as Battisti, Hirst, Neelin and Jin in relation to similar ICM oscillations to provide insight into the underlying mechanism and parameter

spaces of such models. The model itself has considerable room for experimentation with little additional work required as the ocean model may also be run in a non-linear mode, and additional non-linearities may be easily switched on in the SST equation. Of particular interest might be the effects of a non-linear saturation of temperature in the eastern Pacific whereby the SST anomaly is given a physical maximum or minimum that it cannot exceed. This would prevent the runaway growth of the model at large couplings and may prove to be the equivalent non-linearity that Battisti and Hirst found to be crucial for stable oscillations in their delayed oscillator model. Further investigation of the atmosphere model would also provide insight into the mechanism by which sea surface temperature anomalies in the central Pacific grow and develop, and may provide insight into the observed irregularity of ENSO in nature.

APPENDIX

A The reduced gravity model

The general momentum balance equation for a fluid is the Navier Stokes equation which balances the Lagrangian derivative of fluid velocity ($\mathbf{v}$) with the the pressure gradient force (∇p), fluid viscosities (with viscosity μ) and body forces ($\mathbf{f}$), such as gravity:

$$\rho\left(\frac{\partial \mathbf{v}}{\partial t} + \mathbf{v}.\nabla\mathbf{v}\right) = -\nabla p + \mu\nabla^2\mathbf{v} + \mathbf{f} \tag{A.0.4}$$

Making the hydrostatic approximation and neglecting dissipative terms, the equations may be linearised and written in each vector component on a beta plane:

$$\frac{du}{dt} - \beta yv = -\frac{\partial p}{\partial x} \tag{A.0.5a}$$

$$\frac{dv}{dt} + \beta yu = -\frac{\partial p}{\partial y} \tag{A.0.5b}$$

$$0 = -\frac{\partial p}{\partial z} - g\rho \tag{A.0.5c}$$

With the Continuity equation for an incompressible fluid:

$$\frac{\partial u}{\partial x} + \frac{\partial v}{\partial y} + \frac{\partial w}{\partial z} = 0 \tag{A.0.6}$$

The vertical momentum equation is in hydrostatic balance, thus, at a depth z in a fluid of constant density, the pressure may be found by integrating Equation A.0.5c down from the upper surface where the pressure is taken to be zero:

$$p(z) = g\rho(\eta - z) \tag{A.0.7}$$

Where η is the height of the fluid surface.

In the most simple reduced gravity model, a stratified fluid may be considered to be only two layers having a discrete density difference. The upper layer is 'active' and more buoyant than the lower layer which is stationary and infinitely deep. In the lower layer, the pressure at a depth z may be found by a similar process as above, but this time integrating down from the interface between the layers with the pressure at the upper interface now determined by the depth and density of the upper layer:

$$p_2(z) = \rho_1 g(\eta_0 - \eta_1) + \rho_2 g(\eta_1 - z) \tag{A.0.8}$$

$p_2(z)$ is the pressure in the lower layer at depth z, ρ_1 and ρ_2 are the densities in the upper and lower layer respectively, η_0 is the height of the upper (free) surface and η_1 is the height of the interface between layers. Exploiting the fact that the lower

layer is stationary and thus can have no pressure gradients, Equation A.0.8 may be differentiated with respect to either x or y, then integrated to give:

$$C = \rho_1 g\eta_0 + (\rho_2 - \rho_1)g\eta_1 \tag{A.0.9}$$

Where C is an arbitrary constant and may be set to 0. This relation means that given a constant density contrast between two fluids, the surface height is directly related to the height of the interface between the two fluids. For small density contrasts, it can be seen than $\eta_0 < \eta_1$, thus surface displacements are small compared to thermocline displacements. A 'reduced gravity' g' may be defined:

$$g' = g\frac{(\rho_2 - \rho_1)}{\rho_1} \tag{A.0.10}$$

And the momentum equations describing the motion of the fluid in the upper layer become:

$$\frac{du_1}{dt} - \beta y v_1 = -g'\frac{\partial \eta_1}{\partial x} \tag{A.0.11a}$$

$$\frac{dv_1}{dt} + \beta y u_1 = -g'\frac{\partial \eta_1}{\partial y} \tag{A.0.11b}$$

Where the pressure gradient term in the horizonal momentum equations has been replaced by gradients in the interface displacement using Equation A.0.9.

The kinematic condition that $w = d\eta/dt$ may be written for the layer:

$$\frac{\partial w_1}{\partial z} = \frac{\partial}{\partial z}\left(\frac{d\eta_0}{dt} - \frac{d\eta_1}{dt}\right) \tag{A.0.12}$$

So the Continuity equation integrated over the layer becomes:

$$\frac{d}{dt}\left(\eta_0 - \eta_1\right) = -h\left(\frac{\partial u_1}{\partial x} + \frac{\partial v_1}{\partial y}\right) \tag{A.0.13a}$$

$$\frac{dh}{dt} + h\left(\frac{\partial u_1}{\partial x} + \frac{\partial v_1}{\partial y}\right) = 0 \tag{A.0.13b}$$

Equations A.0.11 and A.0.13b form a complete set of equations for determining the motions in the upper layer of a stratified fluid, and it can be seen that they are the same as those for a single layer homogeneous fluid except that the gravity, g, is replaced by a reduced gravity g' which accounts for the denser bottom layer. As such, the shallow water waves such as Kelvin and Rossby waves are admitted by a stratified fluid, and their characteristics are changed compared to a homogeneous layer by the reduced gravity parameter.

B A numerical solution to the Gill model

B.1 Solution proceedure

The governing momentum equations for the atmosphere may be linearised about a mean zonal flow, $\bar{U}$ and non-dimensionalised to give:

$$\epsilon u + \bar{U}u_x - \frac{1}{2}yv = -p_x \tag{B.1.1a}$$

$$\epsilon v + \bar{U}v_x + \frac{1}{2}yu = -p_y \tag{B.1.1b}$$

$$\epsilon p + \bar{U}p_x + u_x + v_y = -Q \tag{B.1.1c}$$

Where for simplicity the momentum and heat dissipation rates are set to be equal, having a non-dimensional inverse time scale ϵ. The variables are non-dimensionalised using:

$$(x^*, y^*) = (c_a/2\beta)^{1/2}(x, y), \quad t^* = (2\beta c_a)^{-1/2}t$$

Where β is the gradient of the Coriolis parameter, and c_a is the characteristic velocity of a mode having an equivalent atmospheric depth of H_a where $c_a = \sqrt{(}gH_a)$. Following Zebiak [1982], an equivalent depth of $400m$ was chosen, corresponding to a Kelvin wave speed of $60ms^{-1}$.

Taking the Fourier Transform in the zonal direction of Equations B.1.1, and defining $\epsilon_1 = \epsilon + ik\bar{U}$, the system becomes:

$$\epsilon_1 U - \frac{1}{2}yV = -ikP \tag{B.1.2a}$$

$$\epsilon_1 V + \frac{1}{2}yU = -P_y \tag{B.1.2b}$$

$$\epsilon_1 P + ikU + V_y = -\bar{Q} \tag{B.1.2c}$$

Which can be expressed in matrix form and solved for the Fourier Transform of meridional velocity using Gaussian elimination. The result is:

$$\left[\left(-\epsilon_1\partial_y + \frac{1}{2}yik\right)\left(\epsilon_1\partial_y + \frac{1}{2}iky\right) + \left(\epsilon_1^2 + \frac{1}{4}y^2\right)(\epsilon_1^2 + k^2)\right]V = \epsilon_1\left(\epsilon_1\partial_y - \frac{1}{2}yik\right)\bar{Q} \tag{B.1.3}$$

Which may be simplified to:

$$V_{yy} + \left[-\frac{1}{4}y^2 + \frac{ik}{2\epsilon_1} - \epsilon_1^2 - k^2\right]V = -\bar{Q}_y + \frac{yik}{2\epsilon_1}\bar{Q} \tag{B.1.4}$$

This may be solved on a grid using finite differences where derivatives are approximated using centered differences:

$$V_{y(i,j)} = \frac{V_{i,j+i} - V_{i,j-1}}{2\Delta y} \tag{B.1.5a}$$

$$V_{yy(i,j)} = \frac{V_{i,j+1} - 2V_{i,j} + V_{i,j-1}}{\Delta y^2} \tag{B.1.5b}$$

Δy is the grid size in the meridional direction.

Equation B.1.4 may be written in a simple form:

$$V_{yy} + AV = B \tag{B.1.6}$$

Where A and B are coefficients defined by B.1.4 which may be evaluated at each grid point. In finite difference form, the equation now becomes:

$$\frac{1}{\Delta y^2}(V_{i,j+1} + (A\Delta y^2 - 2)V_{i,j} + V_{i,j-1}) = B \tag{B.1.7}$$

Writing this equation for each grid point in a meridional column yields a system of simultaneous equations which may be written as a tridiagonal matrix:

$$\begin{bmatrix} \frac{A_{i,1}\Delta y^2-2}{\Delta y^2} & \frac{1}{\Delta y^2} & 0 & \cdots & 0 \\ \frac{1}{\Delta y^2} & \frac{A_{i,2}\Delta y^2-2}{\Delta y^2} & \frac{1}{\Delta y^2} & & \vdots \\ 0 & \ddots & \ddots & \ddots & 0 \\ \vdots & & \frac{1}{\Delta y^2} & \frac{A_{i,M-1}\Delta y^2-2}{\Delta y^2} & \frac{1}{\Delta y^2} \\ 0 & \cdots & 0 & \frac{1}{\Delta y^2} & \frac{A_{i,M}\Delta y^2-2}{\Delta y^2} \end{bmatrix} \begin{bmatrix} V_{i,1} \\ V_{i,2} \\ \vdots \\ V_{i,M-1} \\ V_{i,M} \end{bmatrix} = \begin{bmatrix} B_{i,1} - \frac{1}{\Delta y^2}V_{i,0} \\ B_{i,2} \\ \vdots \\ B_{i,M-1} \\ B_{i,M} - \frac{1}{\Delta y^2}V_{i,M+1} \end{bmatrix} \tag{B.1.8}$$

Boundary conditions of no meridional flow at the upper and lower meridional boundaries are specified by $V_{i,0} = 0$ and $V_{i,M+1} = 0$. Sparse systems of linear equations such as these may be solved using efficient matrix solver algorithms such as the Thomas algorithm (see e.g. Ferziger and Peric [2002]).

Having solved for V, Equations B.1.2a and B.1.2c may be combined to give:

$$(k^2 + \epsilon_1^2)U = \frac{1}{2}\epsilon_1 yV + ikV_y + ik\bar{Q} \tag{B.1.9}$$

So that the Fourier Transform of the zonal velocity may be found by finite differencing the meridional velocity.

The final step of the proceedure is to inverse Fourier Transform U and V and obtain the velocity anomalies u and v in the spatial domain.

B.2 Code: Gill atmosphere model

$N = 86$
$M = 61$
$pi = 2 * \arccos(0.)$
$ci = cmplx(0., 1.)$
$epsilon = 0.3$
$rks = 3.6e - 3$
$u\_bar = 0.$
$qfac = 0.031$
$bet = 1.6e + 3$

non-dimensionalising parameters
$beta0 = 2. * 2. * pi * (1./(24. * 3600.))/6.378e + 6$
$c0 = (9.8 * 400.)**0.5$

domain size in degrees
$L = 168.$
$H = 59.$

domain size in metres
$L = L * 6.378e + 6 * pi/180.$
$H = H * 6.378e + 6 * pi/180.$
$dx = L/(real(N) - 1.)$
$dy = H/(real(M) - 1.)$

non-dimensionalising
$L = ((2. * beta0/c0)**.5) * L$
$H = ((2. * beta0/c0)**.5) * H$
$dx = ((2. * beta0/c0)**.5) * dx$
$dy = ((2. * beta0/c0)**.5) * dy$
$u\_bar = u\_bar/c0$
$u\_barps = u\_barps/c0$
$v\_barps = v\_barps/c0$
$qfac = qfac/(((2. * beta0 * c0)**0.5) * (c0**2.))$
$bet = bet/(c0**2)$
$kfac = 2. * pi/L$

work out array for k
for $j = 1$ to N **do**
  $x(j) = dx * (real(j) - 1.)$
  if $j < ((real(N)/2.) + 1.))$ **then**
    $k(j) = kfac * (real(j) - 1.)$
  else
    $k(j) = kfac * ((-real(N) - 1.) + real(j))$

end if
end for

create low bandpass filter
$kc = 0.75 * kfac * (real(N)/2.)$
for $j = 1$ to N **do**
if abs(k(j)) ¡ kc **then**
$fil(j) = 1.$
else
$fil(j) = \exp(-40. * (k(j) - kc)**4.)$
end if
end for

work out array for y
for $i = 1$ to M **do**
$y(i) = -H/2. + dy * (real(i) - 1.)$
end for

turn sst anomalies into a complex array
$dt\_complex = 0.$
$dt = cmplx(transpose(dt\_real), transpose(dt\_complex))$

calculate diabatic heating using background SSTs, t_bar
$qsst = qfac * dt * \exp((t\_bar - 31.)/17.3)$

calculate convergence of background winds using climatological wind speeds, u_barps and v_barps
for $i = 2$ to $M - 1$ **do**
for $j = 2$ to $N - 1$ **do**
$dudxm(i, j) = (u\_barps(i, j + 1) - u\_barps(i, j - 1))/((2. * dx))$
$dvdym(i, j) = (v\_barps(i + 1, j) - v\_barps(i - 1, j))/((2. * dy))$
end for
end for
for $i = 1$ to M **do**
$dudxm(i, 1) = dudxm(i, 2)$
$dudxm(i, N) = dudxm(i, N - 1)$
end for
for $j = 1$ to N **do**
$dvdym(1, j) = dvdym(2, j)$
$dvdym(M, j) = dvdym(M - 1, j)$
end for
$divm = dudxm + dvdym$
$bgconv = -mask1 * divm$

MAIN LOOP

set parameters for iterative latent heating part
$usoln1 = 0.$
$q1 = 0.$

set maximum number of allowed iterations to be 20
for $iti = 1$ to 20 **do**
  if $iti = 1$ **then**
    for first iteration of each timestep use latent heating term from previous timestep
    $q0 = qsst + qwind$
  else
    $q0 = qsst$
  end if
  $th = q0 + q1$
  fourier transform sst array in x direction
  for $i = 1$ to M **do**
    for $j = 1$ to N **do**
      $throw(j) = th(i, j)$
    end for
    call dfftw_plan_dft_1d $(plan, N, throw, thfftrow, FFTW\_FORWARD,$
                $FFTW\_ESTIMATE)$
    call dfftw_execute $(plan)$
    call dfftw_destroy_plan $(plan)$
    for $j = 1$ to N **do**
      $thfft(i, j) = fil(j) * thfftrow(j)$
    end for
  end for

  compute solutions for atmospheric velocities
  1. calculate coefficients A and B for tridiagonal matrix

  for $j = 1$ to N **do**
    $epsilon1(j) = epsilon + ci * k(j) * u\_bar$
  end for
  for $j = 1$ to N **do**
    for i = 1 to M **do**
      $A(i, j) = -0.25*(y(i)**2.)+(ci*k(j))/(2.*epsilon1(j))-epsilon1(j)**2.-k(j)**2.$
      if i = 1 **then**
        $dqdy(i, j) = (thfft(i + 1, j) - 0.)/(2. * dy)$
      else if i = M **then**
        $dqdy(i, j) = (0 - thfft(i - 1, j))/(2. * dy)$
      else

```
      dqdy(i,j) = (thfft(i+1,j) - thfft(i-1,j))/(2.*dy)
    end if
    B(i,j) = -dqdy(i,j) + ((ci*k(j)*y(i))/(2.*epsilon1(j)))*thfft(i,j)
  end for
end for

2. solve 1 tridiagonal system per column using Simon's tridiagonal
solver
central diagonal: (A(i,j)*dy**2. -2)/(dy**2.)
outer diagonals: 1/dy**2.
for j = 1 to N do
  for i = 1 to M do
    A_col(i) = A(i,j)
    B_col(i) = B(i,j)
  end for
  am = 1./(dy**2.)
  bm = (A_col*(dy**2.) - 2.)/(dy**2.)
  cm = 1./(dy**2.)
  call cthomas_src(M, am, bm, cm, B_col, vsolnft_col)
  for i = 1 to M do
    vsolnft(i,j) = vsolnft_col(i)
  end for
end for

3. solve for zonal velocity
for j = 1 to N do
  for i = 1 to M do
    if i = 1 then
      dvsolndy = (vsolnft(i+1,j) - 0.)/(2.*dy)
    else if i=M then
      dvsolndy = (0 - vsolnft(i-1,j))/(2.*dy)
    else
      dvsolndy = (vsolnft(i+1,j) - vsolnft(i-1,j))/(2.*dy)
    end if
    usolnft(i,j) = (0.5*epsilon1(j)*y(i)*vsolnft(i,j) + ci*k(j)*dvsolndy
                    + ci*k(j)*thfft(i,j))/(k(j)**2. + epsilon1(j)**2.)
  end for
end for

reverse fourier transform velocity fields
for i=1 to M do
  for j = 1 to N do
    vsolnft_row(j) = vsolnft(i,j)
    usolnft_row(j) = usolnft(i,j)
  end for
```

```
    call dfftw_plan_dft_1d (plan, N, vsolnft_row, vsoln_row, FFTW_BACKWARD,
                            FFTW_ESTIMATE)
    call dfftw_execute (plan)
    call dfftw_destroy_plan (plan)
    call dfftw_plan_dft_1d (plan, N, usolnft_row, usoln_row, FFTW_BACKWARD,
                            FFTW_ESTIMATE)
    call dfftw_execute (plan)
    call dfftw_destroy_plan (plan)
    for j = 1 to N do
      vsoln(i, j) = vsoln_row(j)
      usoln(i, j) = usoln_row(j)
    end for
  end for

  renormalise
  usoln = usoln/real(N)
  vsoln = vsoln/real(N)

  find difference between previous iteration
  diff = usoln1 − usoln

  test to see if solution is sufficiently converged
  if (maxval(abs(real(diff))) < 1.e-2) goto 1
  usoln1 = usoln

  compute anomalous divergence of wind field
  for i = 2 to M − 1 do
    for j = 2 to N − 1 do
      dudx(i, j) = (real(usoln(i, j + 1)) − real(usoln(i, j − 1)))/(2. ∗ dx)
      dvdy(i, j) = (real(vsoln(i + 1, j)) − real(vsoln(i − 1, j)))/(2. ∗ dy)
    end for
  end for
  for i = 1 to M do
    dudx(i, 1) = dudx(i, 2)
    dudx(i, N) = dudx(i, N − 1)
  end for
  for j = 1 to N do
    dvdy(1, j) = (real(vsoln(2, j)) − 0.)/(2. ∗ dy)
    dvdy(M, j) = (0. − real(vsoln(M − 1, j)))/(2. ∗ dy)
  end for
  div = dudx + dvdy

  compute new atmospheric heating term
  anomconv = −div
```

```
   totconv = anomconv + bgconv
   for i = 1 to M do
     for j = 1 to N do
       if divm(i,j) + div(i,j) > 0. then
         if divm(i,j) > 0. then
           q1(i,j) = 0.
         else
           q1(i,j) = bet * divm(i,j)
         end if
       else
         if divm(i,j) > 0. then
           q1(i,j) = -bet * (divm(i,j) + div(i,j))
         else
           q1(i,j) = -bet * div(i,j)
         end if
       end if
     end for
   end for
   q1 = mask * q1
end for
PRINT 'did not converge'
1 PRINT 'converged, iteration', iti, it
qwind = q1
vsoln = mask * vsoln
usoln = mask * usoln
u_barps = mask * c0 * u_barps
v_barps = mask * c0 * v_barps

compute total pseudostresses using mean velocity fields
spt = ((real(usoln) + u_barps)**2. + (real(vsoln) + v_barps)**2.)**0.5
sxot = spt * (real(usoln) + u_barps)
syot = spt * (real(vsoln) + v_barps)

compute mean pseudostresses using mean fields
spm = (u_barps**2. + v_barps**2)**0.5
sxom = spm * u_barps
syom = spm * v_barps

anomalous pseudostress is just the difference
sxoa = rks * (sxot - sxom)
syoa = rks * (syot - syom)

END
```

C Parameters used in the 'standard run'

Parameter name	Symbol	Value
Atmospheric parameters		
Diabatic heating	α	$0.31 m^2 s^{-3}/^{\circ}C$
Latent heating	β	1.6 x $10^3 m^2 s^{-2}$
Kelvin wave speed	c_a	$60 ms^{-1}$
Friction	ϵ	$(2 \text{ days})^{-1}$
Oceanic parameters		
Thermocline depth	H	$150m$
Kelvin wave speed	c	$2.2 ms^{-1}$
Biharmonic diffusion of height	rnuhoc	2000
Biharmonic viscosity	rnumoc	20000
Ratio densities between layers	$\Delta\rho/\rho_0$	0.00329
SST equation parameters[1]		
Thermal dissipation timescale	$\gamma_{sst}(x)$	$(60 \text{ days})^{-1}$ - $(14.77 \text{ days})^{-1}$
Thermocline height factor	$\alpha_{sst}(x)$	0.17 - 1.6 $K(10m)^{-1} month^{-1}$
Horizontal advection factor	$\beta_{sst}(x)$	0.0 - 1.0 $K(0.1Pa)^{-1} month^{-1}$
Other miscellaneous parameters		
Model timestep	T	$1/3 day$
Drag coefficient	ζ	3.6 x 10^{-3}

[1] Values expressed as a range due to variation in values across basin

D Monthly wind fields

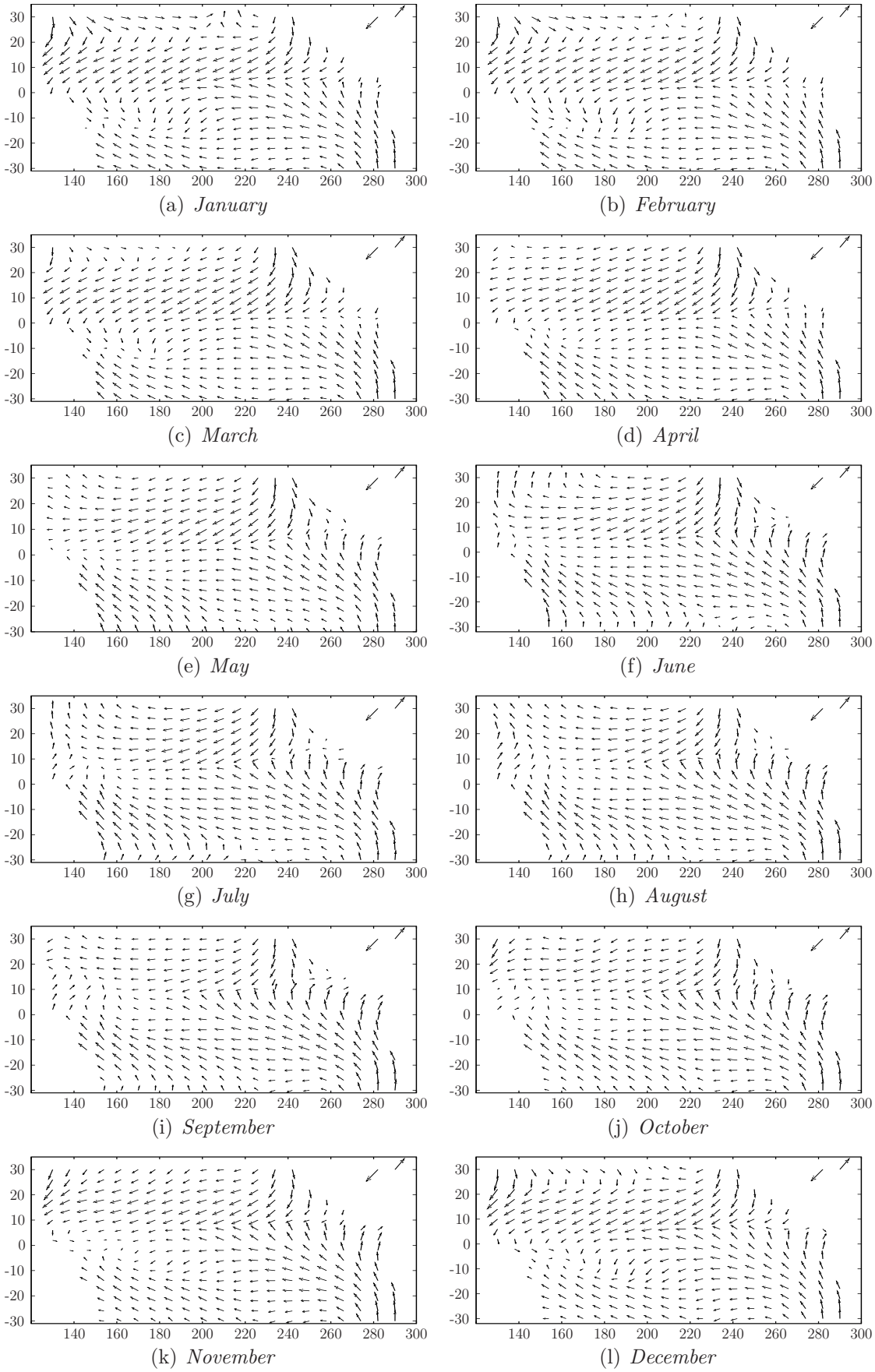

(a) *January* (b) *February*

(c) *March* (d) *April*

(e) *May* (f) *June*

(g) *July* (h) *August*

(i) *September* (j) *October*

(k) *November* (l) *December*

Figure 17: *Background winds. Arrows in top right demostrate scale and have magnitudes* $9.75ms^{-1}$ *(directed north-east) and* $11.6ms^{-1}$ *(directed south-west).*

E Monthly wind speeds

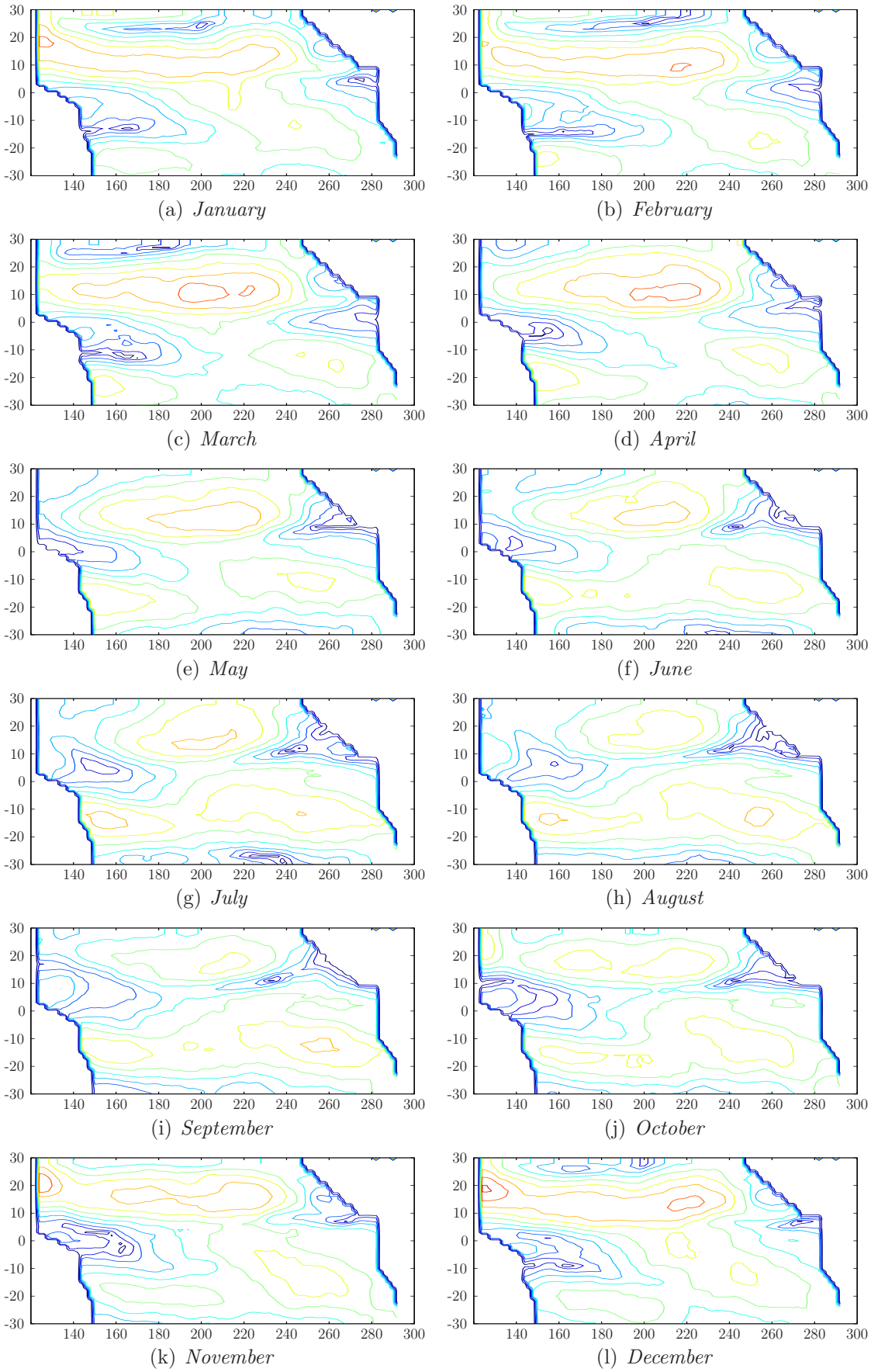

(a) *January* (b) *February*

(c) *March* (d) *April*

(e) *May* (f) *June*

(g) *July* (h) *August*

(i) *September* (j) *October*

(k) *November* (l) *December*

Figure 18: *Background wind speed climatologies. Each contour is 1ms^{-1} with an overall maximum of 12ms^{-1} and a minimum of 0ms^{-1}*

F Monthly wind field convergence climatologies

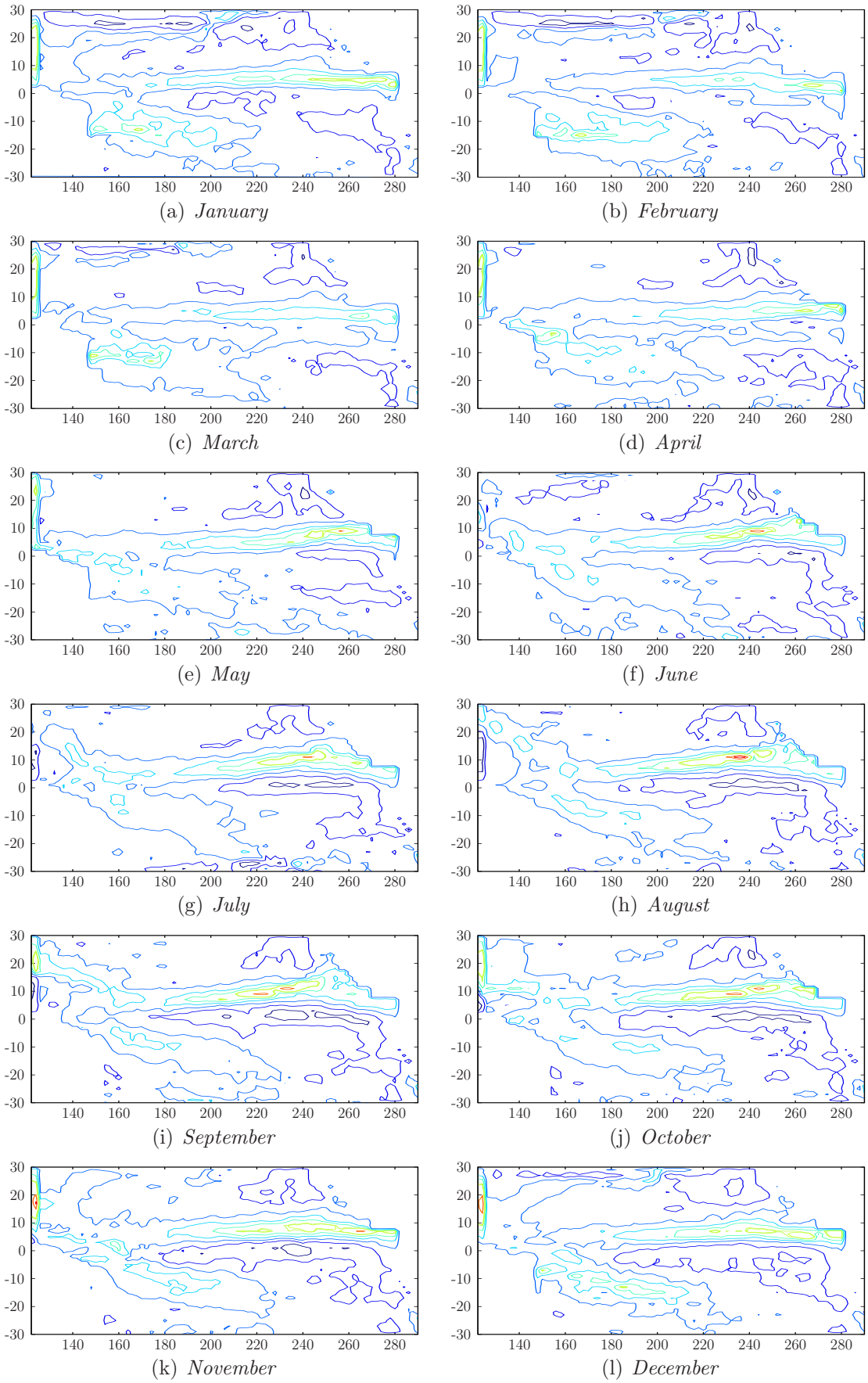

(a) *January* (b) *February*

(c) *March* (d) *April*

(e) *May* (f) *June*

(g) *July* (h) *August*

(i) *September* (j) *October*

(k) *November* (l) *December*

Figure 19: *Background wind convergence climatologies. Each contour is 0.063ms^{-2} with an overall maximum of 0.46ms^{-2} and a minimum of -0.17ms^{-2}*

G Monthly SST climatologies

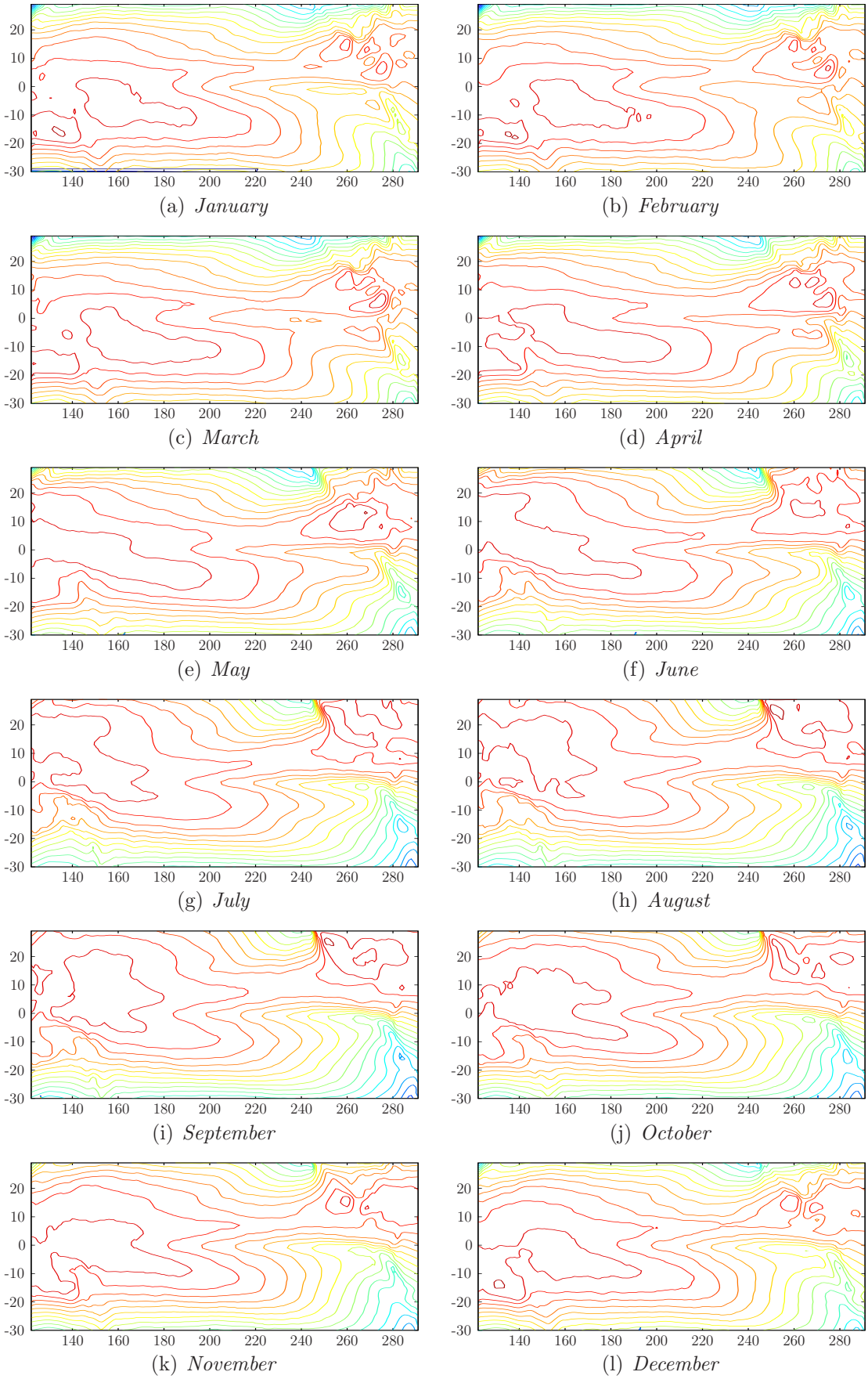

(a) *January* (b) *February*

(c) *March* (d) *April*

(e) *May* (f) *June*

(g) *July* (h) *August*

(i) *September* (j) *October*

(k) *November* (l) *December*

Figure 20: *SST climatologies, each contour is 1° with an overall maximum of 31° and a minimum of 10°*

References

David S. Battisti and Anthony C. Hirst. Interannual variability in a tropical atmosphere-ocean model: Influence of the basic state, ocean geometry and nonlinearity. *Journal of the Atmospheric Sciences*, 46:1687–1712, 1988.

J.-P. Boulanger. The Trident Pacific model. part 1: Simulating surface ocean currents with a linear model during the 1993-1998 TOPEX/POSEIDON period. *Climate Dynamics*, 17:159–173, 2001.

Gerrit Burgers and Geert Jan Van Oldenborgh. On the impact of local feedbacks in the central pacific on the ENSO cycle. *Journal of Climate*, 16:2396–2407, 2003.

Gerrit Burgers, Magdalena A. Balmaseda, Femke C. Vossepoel, Geert Jan Van Oldenborgh, and Peter Jan Van Leeuwen. Balanced ocean-data assimilation near the Equator. *Journal of Physical Oceanography*, 32:2509–2519, 2002.

Simon R. Clarke. Fortran code for solving a complex tridiagonal matrix.

Gregory T Cushman. Enclave vision: Foreign networks in Peru and the internationalization of El Niño research during the 1920s. In *Proc. of the International Commission on History of Meteorology 1.1*, 2004.

Henk A. Dijkstra. *Nonlinear Physical Oceanography: A Dynamical Systems Approach to the Large Scale Circulation and El Niño*. Spinger, second edition, 2005.

Henk A. Dijkstra and Gerrit Burgers. Fluid dynamics of El Niño variability. *Annu. Rev. Fluid Mech.*, 34:531–58, 2002.

J. H. Ferziger and M. Peric. *Computational Methods for Fluid Dynamics*. Springer, 2002.

A.E. Gill. Some simple solutions for heat-induced tropical circulation. *Quarterly Journal for the Royal Meteorological Society*, 106:447–462, 1980.

Anthony C. Hirst. Unstable and damped equatorial modes in simple coupled ocean-atmosphere models. *Journal of the Atmospheric Sciences*, 43:606–630, 1985.

Fei-Fei Jin and J.David Neelin. Modes of interannual tropical ocean - a unified view, I, numerical results. *Journal of the Atmospheric Sciences*, 50:3477–3503, 1993a.

Fei-Fei Jin and J.David Neelin. Modes of interannual tropical ocean - a unified view, II, analytic results in the weak-coupling limit. *Journal of the Atmospheric Sciences*, 50:3504–3522, 1993b.

Fei-Fei Jin and J.David Neelin. Modes of interannual tropical ocean - a unified view, III, analytic results in fully coupled cases. *Journal of the Atmospheric Sciences*, 50:3523,3540, 1993c.

J.David Neelin. The slow sea surface temperature mode and the fast-wave limit: Analytic theory for tropical interannual oscillations and experiments in a hybrid coupled model. *Journal of the Atmospheric Sciences*, 48:584–606, 1990.

Joseph Pedlosky. *Geophysical Fluid Dynamics*. Springer, 1986.

T. M. Smith R. W. Reynolds. Improved global sea surface temperature analyses. *Journal of Climate*, 7:929–948, 1994.

Max J. Suarez and Paul S. Schopf. A delayed action oscillator for ENSO. *Journal of the Atmospheric Sciences*, 45:3283–3287, 1988.

Stephen E. Zebiak. A simple atmoshpheric model of relevance to El Niño. *Journal of the Atmospheric Sciences*, 39:2017–2027, 1982.

Stephen E. Zebiak. Atmospheric convergence feedback in a simple model for El Niño. *Monthly Weather Review*, 114:1263–1271, 1986.

Stephen E. Zebiak and Mark A. Cane. A model El Niño-Southern Oscillation. *Monthly Weather Review*, 115:2262–2278, 1987.